

Electronic Thesis and Dissertation Repository

2-23-2015 12:00 AM

Neural Correlates of Spontaneous BOLD Fluctuations: A Simultaneous LFP-fMRI Investigation In The Non-human Primate

Masoomeh Hashemi
University of Western Ontario

Supervisor
Dr. Stefan Everling
The University of Western Ontario

Graduate Program in Neuroscience
A thesis submitted in partial fulfillment of the requirements for the degree in Master of Science
© Masoomeh Hashemi 2015

Follow this and additional works at: <https://ir.lib.uwo.ca/etd>



Part of the [Cognitive Neuroscience Commons](#)

Recommended Citation

Hashemi, Masoomeh, "Neural Correlates of Spontaneous BOLD Fluctuations: A Simultaneous LFP-fMRI Investigation In The Non-human Primate" (2015). *Electronic Thesis and Dissertation Repository*. 2802.
<https://ir.lib.uwo.ca/etd/2802>

This Dissertation/Thesis is brought to you for free and open access by Scholarship@Western. It has been accepted for inclusion in Electronic Thesis and Dissertation Repository by an authorized administrator of Scholarship@Western. For more information, please contact wlsadmin@uwo.ca.

NEURAL CORRELATES OF SPONTANEOUS BOLD FLUCTUATIONS: A
SIMULTANEOUS LFP-FMRI INVESTIGATION IN THE NONHUMAN PRIMATE
(Thesis format: Monograph)

by

MASOOMEH HASHEMI

Graduate Program in Neuroscience

A thesis submitted in partial fulfillment
of the requirements for the degree of
Master of Science

The School of Graduate and Postdoctoral Studies
The University of Western Ontario
London, Ontario, Canada

© Masoomeh Hashemi 2015

Abstract

Resting-state functional magnetic resonance imaging (rs-fMRI) is widely used to explore functional connectivity (FC) between brain regions across neurological and psychiatric diseases. However, the neural basis of spontaneous low frequency blood-oxygen level dependent (BOLD) fluctuations is poorly understood.

Here, we acquired rs-fMRI data in macaque monkeys together with simultaneous recordings of local field potentials (LFPs) in prefrontal cortex area 9/46d. We first evaluated the correlation between LFPs (1-100 Hz) and BOLD signals and found unique frequency power correlates of positive and negative FC. Anti-correlation of high and low power envelopes indicated that ongoing cross-frequency interactions are a neural correlate of FC. On the other hand, seed-based analysis of the BOLD signal from the vicinity of electrode revealed the same spatial topology when using the power envelopes of high frequency bands of LFPs in the regression analysis.

Variations of the canonical hemodynamic response function (HRF) in distinct cortical areas were also investigated to find the optimal HRF that can best fit in model analysis and estimate the BOLD response. While we found the optimal HRF that yields the highest correlation, the HRF shape was consistent within subjects and between brain regions.

Our results suggest that intrinsic connectivity networks may be specifically driven by unique LFP profiles and these profiles contribute differently to BOLD FC. This study provides insight into the neural correlates of spontaneous BOLD FC at rest.

Keywords: rs-fMRI, Local Field Potential, Simultaneous Recording

To my parents, Monireh Mahjobnia and AhmadAli Hashemi, whose words of encouragement ring in my ears.

Acknowledgments

I would like to extend my thanks and my appreciation to everyone who has aided and supported me throughout the extent of my thesis. Foremost, I would like to thank my supervisor Dr. Stefan Everling, who provided guidance and mentorship throughout the entirety of the project. Through working with him the past two years, I have grown considerably as a scientist. Coming with an engineering background, next I extend a special thanks to Dr. Kevin Johnston who at the beginning of my master's program gave me the opportunity to develop my knowledge on the fundamental principles of neuroscience and also for his acknowledgement in performing the surgeries necessary for my experiments.

I would also like to thank the members of my advisory committee, Dr. Ravi Menon and Dr. Rhodri Cusack and also our MRI engineer, Joe Gati. Ravi and Joe helped a lot with fMRI scanning procedures and provided thoughtful feedback each time that led to substantial improvements. Rhodri always took the time to provide me with invaluable insights and tirelessly read and re-read this thesis.

I express my sincere appreciation specifically to Matt Hutchison for his expertise in functional magnetic resonance imaging and data analysis and also for reading my long emails and answering all of my endless questions.

Darren Pitre and Nicole Hague are two amazing people who taught me a lot about animal care and handling. Their dedication to work and their love for monkey world always inspired me. Nicole invariably contributed to all the surgeries and scanning sessions and she has allowed the project to move forward smoothly. My thanks are also towards Kevin Barker with his mechanical engineering expertise, who saved us a lot of time and energy and made

working with animals more enjoyable.

Having all these great supervision would not be possible to complete this academic journey if I did not have a wonderful working environment. Everling lab members were such encouraging lab mates that continuously supported me like how friends do. Thanks to all of them for creating such a comfortable environment and thanks to my friends who walked beside me on this path.

I am grateful to my aunt Mahboubeh Mahjoubnia and my uncle Ramin Khorshid who helped me in every stage of moving to Canada to continue my education and supported me in every way while being here. Most importantly, my parents and my only sister Narges deserve special thanks for always believing in me. With their unconditional love, I never thought I am miles away from them, from home.

Table of Contents

| | |
|---|------|
| Abstract..... | ii |
| Acknowledgments | iv |
| Table of Contents | vi |
| List of Figures..... | viii |
| List of Appendices..... | x |
| List of Abbreviations and Symbols | xi |
| 1 Introduction..... | 1 |
| 1.1 Resting-state functional Magnetic Resonance Imaging in the Clinical Realm | 1 |
| 1.2 How fMRI Works..... | 2 |
| 1.3 Resting-State fMRI..... | 6 |
| 1.3.1 Resting-State Functional Connectivity..... | 7 |
| 1.3.2 Structural vs Functional Connectivity | 8 |
| 1.4 fMRI-based Approaches for Identifying Spatial Patterns | 9 |
| 1.5 Contribution of Electrophysiology to fMRI | 10 |
| 1.6 HRF Models for fMRI Data Analysis | 11 |
| 1.7 Neural Basis of BOLD fMRI | 12 |
| 1.7.1 Single-Unit Recordings | 14 |
| 1.7.2 Multi-Unit Recordings..... | 14 |
| 1.7.3 Local Field Potentials..... | 15 |
| 1.7.4 BOLD Signal Is A Reflection of Synaptic Activity | 16 |
| 1.7.5 How to Study Local Field Potentials..... | 18 |
| 1.8 Microcircuitry Differences across the Cortex | 18 |
| 1.9 Human and Monkey Brain Similarities..... | 20 |
| 1.10 Neural Correlates of Resting-state BOLD fMRI | 21 |

| | |
|--|----|
| 1.11 Rationale and Hypothesis of the Current Study | 24 |
| 2 Methods | 26 |
| 2.1 Animal Implantation..... | 26 |
| 2.2 Animal Preparation..... | 28 |
| 2.3 MRI Acquisition..... | 29 |
| 2.4 LFP Acquisition..... | 30 |
| 2.5 Image Preprocessing..... | 32 |
| 2.6 BOLD-fMRI Analysis..... | 33 |
| 2.7 LFP Analysis | 35 |
| 3 Results..... | 38 |
| 3.1 BOLD Seed-Based Analysis | 38 |
| 3.2 LFP-BOLD Correlation..... | 40 |
| 3.2.1 LFP-BOLD Correlation within Averaged BOLD Networks..... | 40 |
| 3.2.2 LFP-BOLD Correlation within Individual ROIs..... | 43 |
| 3.3 Effect of HRF Variation on LFP-BOLD Correlation..... | 45 |
| 3.4 Electrophysiological BLP Regression Analysis..... | 53 |
| 4 Discussion and Conclusions | 58 |
| 4.1 LFP-BOLD Correlation..... | 58 |
| 4.2 Effect of HRF Variation on LFP-BOLD Correlation..... | 61 |
| 4.3 Resting-State fMRI Confounds | 62 |
| 4.4 Effect of Anesthetics on Brain Functional Architecture | 64 |
| 4.5 Conclusions | 64 |
| References | 67 |
| Appendix A | 85 |
| Curriculum Vitae | 86 |

List of Figures

| | |
|---|----|
| Figure 1: HRF Model..... | 6 |
| Figure 2: Recording Electrophysiological Signals With Different Techniques..... | 21 |
| Figure 3: Electrode Placement from Different Views..... | 27 |
| Figure 4: Hardware and Connection setup..... | 31 |
| Figure 5: LFP Signal Representation During 1s Scanning..... | 32 |
| Figure 6: Functional Images of Monkey 2 overlaid on F99 Template..... | 34 |
| Figure 7: Signal-to-Noise Ratio Map of Monkey 2..... | 34 |
| Figure 8: LFP Analysis Pipeline..... | 37 |
| Figure 9: Spontaneous BOLD connectivity networks of Monkey 1..... | 39 |
| Figure 10: Correlation of BLP 5Hz bins with Average BOLD Network Time Series..... | 41 |
| Figure 11: BLP-LFP BOLD Correlation of Contact Electrodes on Monkey 2..... | 42 |
| Figure 12: Convolved BLP-LFP BOLD Correlation at FEF and Area 7m..... | 44 |
| Figure 13: Effect of HRF Variation on LFP-BOLD Correlation for Averaged Positive BOLD Networks in Monkey 1..... | 47 |
| Figure 14: Effect of HRF Variation on LFP-BOLD Correlation for Averaged Positive BOLD Networks in Monkey 2..... | 48 |
| Figure 15: Effect of HRF Variation on LFP-BOLD Correlation for FEF area in Monkey 1..... | 49 |
| Figure 16: Effect of HRF Variation on LFP-BOLD Correlation for area 7m in Monkey 2..... | 50 |
| Figure 17: Effect of Automatic HRF Variation on LFP-BOLD Correlation for Averaged Positive BOLD Networks in Both Monkeys..... | 51 |

| | |
|--|----|
| Figure 18: Optimized Values for Delay and Dispersion of the Peak. | 52 |
| Figure 19: Representative Traces of BOLD, High BLP-LFP and Low BLP-LFP. | 53 |
| Figure 20: Electrophysiological High BLP Regression Analysis. | 54 |
| Figure 21: Electrophysiological Low BLP Regression Analysis. | 55 |
| Figure 22: Electrophysiological BLP Regression Analysis on Surface Maps for Monkey 1. | 56 |
| Figure 23: Electrophysiological BLP Regression Analysis on Surface Maps for Monkey 2. | 57 |

List of Appendices

| | |
|-----------------|----|
| Appendix A..... | 85 |
|-----------------|----|

List of Abbreviations and Symbols

| | |
|-----------------|--|
| AP | action potential |
| ADHD | attention deficit hyperactivity disorder |
| ATP | adenosine-triphosphate |
| BLP | band limited power |
| BOLD | blood-oxygen level dependent |
| CCM | canonical cortical microcircuitry |
| CBF | cerebral blood flow |
| CBV | cerebral blood volume |
| CO ₂ | carbon dioxide |
| CO | carbon monoxide |
| CSD | current source density |
| CSF | cerebral spinal fluid |
| dHb | deoxyhemoglobin |
| DMN | default mode networks |
| DOF | degrees of freedom |
| ECOG | electrocorticography |
| EEG | electroencephalography |
| EPI | echo planar imaging |
| EFP | extracellular field potential |
| EPSP | excitatory postsynaptic potential |
| FEF | frontal eye field |
| fMRI | functional magnetic resonance imaging |
| FSL | FMRIB Software Library |
| GBA | gamma band activity |

| | |
|-----------------|-------------------------------------|
| GLM | general linear model |
| GSR | global signal regression |
| Hb | hemoglobin |
| HRF | hemodynamic response function |
| ICA | independent-component analysis |
| ICM | intrinsic coupling mode |
| IPSP | inhibitory postsynaptic potential |
| L4 | layer 4 |
| LFP | local field potential |
| MC | motion correction |
| mEFP | mean extracellular field potentials |
| MEA | multi electrode arrays |
| MS | multiple sclerosis |
| MUA | multi unit activity |
| Na ⁺ | sodium |
| PET | positron emission tomography |
| rCBV | regional cerebral blood volume |
| RF | radio frequency |
| ROI | region of interest |
| rs | resting-state |
| RSN | resting-state networks |
| SC | structural connectivity |
| SEF | supplementary eye field |
| SNR | signal-to-noise ratio |
| SPM | statistical parametric mapping |

| | |
|------------------|-------------------------|
| SPO ₂ | blood oxygen saturation |
| SUR | single unit recording |
| V1 | primary visual cortex |
| V2 | visual area 2 |
| WM | white mater |

| | |
|-------------------|------------------------|
| B_0 | magnetic field |
| δ | delta |
| θ | theta |
| α | alpha |
| β | beta |
| γ_L | low gamma |
| γ_H | high gamma |
| Hz | hertz (cycles/second) |
| μm | micrometer(s) |
| mm | millimeter(s) |
| cm | centimeter(s) |
| m | meter(s) |
| mm^3 | cubic millimeter(s) |
| ms | millisecond(s) |
| mg | milligram(s) |
| Kg | kilogram(s) |
| min | minute(s) |
| s | second(s) |
| T | Tesla |
| T_1, T_2, T_2^* | time constant |
| II, III, IV, V | two, three, four, five |

1 Introduction

1.1 Resting-state functional Magnetic Resonance Imaging in the Clinical Realm

It has been almost two decades since the first time slow fluctuations in the resting human brain were observed using functional magnetic resonance imaging (fMRI) (Biswal et al., 1995). This technique has now been the focus of neuroscientists who study the brain's functional and anatomical networks as well as relative changes that occur in neurological disorders. Compared to task-based fMRI, which requires subjects to perform a task while being scanned, resting-state fMRI (rs-fMRI) is based on intrinsic activities in the brain. This basis allows the subjects to rest with their eyes open or closed, which can be beneficial for studies in which patients are unable to perform the required tasks, such as stroke patients or Alzheimer's patients.

Among all different neurological disorders being studied by rs-fMRI, epilepsy has gained the most attention for pre-surgical diagnoses that attempt to find the epileptic foci (Zijlmans et al., 2007) and the connectivity alterations (Centeno and Carmichael, 2014; Pereira et al., 2010). Alzheimer's disease (Greicius et al., 2004), depression (Anand et al., 2005), schizophrenia (Bluhm et al., 2007; Zhou et al., 2007), attention deficit hyperactivity disorder (ADHD) (Castellanos et al., 2009; Wang et al., 2009; Yu-Feng et al., 2007) and multiple sclerosis (MS) (Lowe et al., 2002) are other examples of brain disorders under investigation using rs-fMRI.

While early results have been consistent among various studies for some disorders like Alzheimer's disease, there is less reproducibility for other diseases, such as schizophrenia

(Greicius, 2008). To further develop this research field, we must better understand the underlying mechanism of the spontaneous fluctuations in the brain that are recorded by rs-fMRI. This realization can be undertaken by using multimodal approaches, some of which are simultaneous electroencephalography (EEG)-fMRI, electrocorticography (ECOG)-fMRI and local field potential (LFP)-fMRI recording, which is the focus of this thesis.

1.2 How fMRI Works

In 1878, the Italian physiologist, Angelo Mosso, performed the first brain imaging by inventing the human circulation balance. He was recording the pulsation of a human cortex with a plethysmograph when he found out that these pulsations fluctuate as a result of mental activity. He suggested that blood volume in the brain increases when the brain is mentally active. The subject would lay on a balanced table that could tilt either at the head or at the foot if the weight of either end were increased. As soon as an emotional or a mental activity began in the subject the balance tipped toward the head end as an outcome of increase in blood flow to the head (reported in James, 1890). This technique is known to be the predecessor of the more advanced techniques of fMRI and positron emission tomography (PET) (Raichle et al., 2001). The former benefits from the coupling between neuronal activity and hemodynamics (local changes in blood flow and oxygenation) in the brain.

The energy needed for brain function is a product of glucose oxidation to carbon dioxide and water (Fox et al., 1988). There is little dissolved oxygen in brain tissue, as most of it remains bound to hemoglobin in red blood cells. Therefore, the brain is dependent on a continuous supply of oxygen via flowing blood. At rest, oxygen consumption is higher

than glucose consumption. When a visual stimulus is presented, oxygen consumption increases by 5% and glucose consumption by 51%. Therefore, the excessive amount of glucose, which is not converted to energy, is metabolized to lactate (Fox et al. 1988). This increase implies that the amount of extra energy used in the brain during conscious information processing is small compared to resting-state energy consumption (Schölvinck et al., 2008) demonstrating how important it is to investigate spontaneous activity in the resting brain.

Compared to oxygenated hemoglobin (Hb), deoxyhemoglobin (dHb) is paramagnetic and when it is placed in a strong magnetic field, like an MRI scanner, dHb disrupts the magnetic field, while Hb does not (Pauling and Coryell, 1936). Therefore, draining veins will show up dark in MRI images due to signal loss that is caused by inhomogeneity in the magnetic field. When cellular activity in an area of the brain is enhanced, cerebral blood flow (CBF), cerebral blood volume (CBV) and, as a result, oxygenated Hb in the capillaries and veins increase. In 1990, Ogawa and colleagues showed that this would in fact lead to a rise in the fMRI signal, which was named blood oxygenation level dependent (BOLD) contrast (Ogawa et al., 1990). The fMRI response that results from a short local neuronal activity is called hemodynamic response function (HRF) (Heeger and Ress, 2002; Logothetis, 2002). Although, these principles have been known for some time now, the exact mechanism underlying the coupling between neuronal activity and CBV and CBF is still unclear.

The brain's vascular system consists of arteries, capillaries and veins that each exist at different spatial scales. Arteries are thick-walled vessels that carry blood away from the heart. The arteries branch into smaller vessels, arterioles, and the arterioles eventually

end in capillaries, small and thin-walled blood vessels. Extraction of oxygen and glucose from the blood and removal of CO₂ happens in the capillaries. The deoxygenated blood is then carried to small veins called venules and these venules collect into the veins. The arterial cerebral circulation is divided into anterior cerebral circulation, which supplies anterior and medial surface of the brain, and posterior cerebral circulation, which supplies posterior part of the brain including occipital lobe, cerebellum and brainstem (Huettel et al., 2004).

The density of vascularization is not uniform across cortical layers. While small arterioles vascularize the gray matter and superficial layers, vessels with larger diameter vascularize the white matter and deep layers. Denser vascularization is observed where the neural cell bodies have higher concentration (Duvernoy et al., 1981).

Changes in neuronal activity result in changes in CBF and CBV in the active area and also in distant areas with no neuronal activation (Iadecola et al., 1997). Although, the vessel dilation happens several millimeters away, it is in a much lower extent compared to the vessel dilation in the activation center. This in fact puts limitation on the spatial resolution of fMRI that depends on hemodynamic changes and part of the solution is spatial smoothing the data image in the preprocessing step.

The shape of the hemodynamic response includes three phases of the BOLD fMRI response to a transient increase in neuronal activity (see Figure 1). The first phase is a small decrease below the baseline that is caused by the initial period of oxygen consumption. This consumption results in an increase in the dHb concentration and is called the initial dip. After about two seconds, there is a large increase in hemodynamic

response above baseline due to an oversupply of oxygenated blood that provides enough glucose but excessive oxygen. At this point, HRF has reached its peak. Finally, when the oversupply of oxygenated blood has diminished, it still takes some time for the blood volume to return to its baseline again by a negative undershoot (Heeger and Ress, 2002).

In regards to the initial dip, it is worth noting that optical imaging studies have shown that this component of the HRF as a result of the increase in oxygen consumption is more correlated to neuronal activity than any other components of the HRF (Jones et al., 2001; Menon et al., 1995). However, the majority of fMRI studies have not reported this initial dip and this in fact is a source of controversy that questions its presence (Buxton, 2001; Logothetis, 2000).

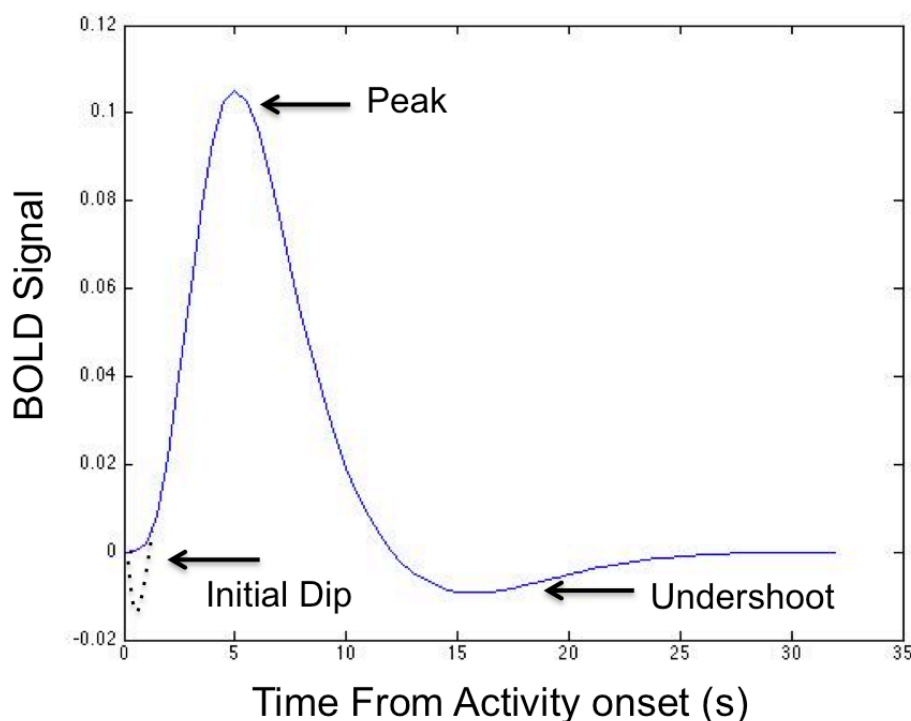


Figure 1: HRF Model. The shape of HRF with its three phases is shown here. Delay of the peak is about 4-6 s and the post-stimulus undershoot appears after about 16 s.

The underlying signal of BOLD comes from hydrogen atoms that exist in large amounts in the water molecules of the brain. With no external magnetic field B_0 , all hydrogen atoms spin along their axes. In the presence of a magnetic field, these hydrogen atoms absorb energy and align with B_0 , while rotating at different phases with the angular frequency of Larmor. When a radio-frequency (RF) pulse is applied, they tip over and their phases realign altogether. After removing the RF pulse, the hydrogen atoms emit energy until they gradually return to equilibrium. This process coincides with the reduction in the transverse magnetization (called transverse relaxation, described by time constant T_2) and growth in the longitudinal magnetization (called longitudinal relaxation, described by time constant T_1) (Huettel et al., 2004).

The MRI scanner measures the sum total of the emitted radio-frequency energy. As mentioned earlier, greater inhomogeneity results in decreased image intensity. The combined effect of transverse decay of magnetization and local inhomogeneity is called T_2^* (Logothetis, 2002). Some MRI pulse sequences are designed to eliminate the inhomogeneity of local magnetic fields, while others are designed to emphasize it within small volumes of tissue. The latter is the basis of BOLD fMRI techniques (Heeger and Ress, 2002).

1.3 Resting-State fMRI

Since 1938 when results from Barenne and McCulloch were published, the large-scale organization of the mammalian brain at rest has been extensively explored. Barenne and McCulloch placed a small amount of strychnine, which is an excitatory agent, on small areas of the sensory cortex of monkey, while the animal was first awake and then anesthetized. Simultaneously, they recorded neural activity in the vicinity of the

stimulated area. They could see similar activation within distant subdivisions of the sensory cortex (Dusser de Barenne and McCulloch, 1938). This method of chemical neuronography was also used by Pribram and MacLean to report five distinct regions of reciprocal excitation in medial and basal cortices of limbic systems (Pribram and MacLean, 1953).

Biswal and colleagues opened a new direction in the large-scale functional connectivity field in 1995. They observed that the patterns of slow fluctuations in the sensory strip and many other regions that are associated with motor function, of the resting human brain are similar to functional activation found in behavioral tasks (Biswal et al., 1995). They also found evidence that similar patterns exist in visual and auditory networks. The instant implication of their findings was that, in order to investigate the basic properties of large-scale networks of the brain, one could study the correlational relationship of spontaneous activity in the absence of a task.

1.3.1 Resting-State Functional Connectivity

Analyzing the spontaneous activities in the absence of stimulus or task distinguishes several specific functional networks. These networks represent high temporal covariation, which became known as resting-state networks (RSN). These networks have been studied in both awake and anesthetized animals such as rats (Hutchison et al., 2010; Liang et al., 2011; Pan et al., 2011; Pawela et al., 2008) and monkeys (Hutchison et al., 2011; Hutchison et al., 2013; Dante Mantini et al., 2011). Human studies also have revealed a set of core RSNs (Beckmann et al., 2005; De Luca et al., 2006; Hutchison et al., 2013). Such networks have been compared across individuals (Biswal et al., 2010) to demonstrate a universal architecture of functional connections.

RSNs have been determined to be consistent across subjects, which is a solid foundation for continuing rs-fMRI investigations (Shehzad et al., 2009). Through the course of development from infancy to adolescence, resting-state functional connectivity (rs-FC) is changed considerably. Meanwhile, several large-scale network properties are shown to be preserved across development. This preservation suggests that rs-FC networks, even in children, are organized in a manner similar to the adult brain (Power et al., 2010).

A number of RSNs have been characterized using fMRI-based methods. Dorsal attention (Laufs et al., 2003), auditory (Cordes et al., 2000), visual (Lowe et al., 1998), executive control and default mode networks (DMN) are some examples (Fox and Raichle, 2007; Raichle, 2010). Regions within DMNs decrease their activity during a task performance and show more activation at rest. This antagonistic network relationship between DMNs and specifically dorsal-attention network regions led to the hypothesis that the brain is active in an organized way at rest (Raichle, 2010).

Like other resting-state networks, DMNs have been shown to be present in different brain states besides awake, such as wandering and sleep in humans, and anesthesia among different species like rats and monkeys (Horovitz et al., 2008; Hutchison et al., 2010; Mason et al., 2007; Pawela et al., 2008; Vincent et al., 2007).

1.3.2 Structural vs Functional Connectivity

It is widely assumed that structural connectivity (SC) and functional connectivity (FC) have strong linkage and it has been reported that FC and SC are correlated at a gross level (Damoiseaux et al., 2006; Passingham et al., 2002). However, the nature of this linkage has been under investigation using fMRI and diffusion tractography. Honey and

colleagues showed that FC (measured with rs-fMRI) exists between regions that do not have direct structural connections (measured with diffusion spectrum imaging tractography (Honey et al., 2009)). They also reported that some of the variance observed in FC could be due to indirect connections and between-regional distance, which results in reduction of both kinds of connections. In summary, SC and FC organizations are significantly related and anatomically connected areas seem to show more consistent FC than unconnected areas (Honey et al., 2007; Hagmann et al., 2008; Honey et al., 2009; Koch et al., 2002; Shen et al., 2012).

1.4 fMRI-based Approaches for Identifying Spatial Patterns

There are several techniques to identify the functionally connected areas in the brain and their spatial patterns. The most commonly used approaches are seed-based analysis, hierarchical clustering and independent-component analysis (ICA).

To conduct a seed-based analysis, first the fMRI-BOLD time course from a region of interest (ROI) is extracted. Then the temporal correlation between this time course and all other voxels in the brain is calculated. Many studies use seed-based analysis because of its simplicity; however, a disadvantage here is that the results are dependent on the *a priori* decision on choosing the seeds. Multiple seeds have to be chosen subsequently in order to determine the temporal correlation between different regions (Fox and Raichle, 2007). On the other hand, hierarchical clustering requires extracting the time courses of multiple seed regions and creating a correlation matrix. A clustering algorithm is used in order to find the most positively or negatively related regions. This technique suffers from the same disadvantage as seed-based analysis (Fox and Raichle, 2007).

ICA benefits from the fact that it is data driven and automatically distinguishes noise from the BOLD data. ICA algorithms analyze the whole data and separate it into several components that are statistically independent of each other and each have a spatial map. Three major downsides of this technique are: 1) its dependency on the number of components one asks the algorithm to produce, 2) its dependency on the user who has to define noise and non-neuronal components, 3) interpretation complexities due to algorithm sophistication.

1.5 Contribution of Electrophysiology to fMRI

Finding the relationship between simultaneous fluctuations in neural activity across different regions of the brain is a key approach to probe brain function (Schölvinck et al., 2013). Beside fMRI, electrophysiology can assess the temporal correlation between the regions as a measure of their functional connections both during a task performance and at rest. Despite, the success of fMRI with its high spatiotemporal resolution compared to EEG and ECOG techniques in brain mapping, the link between hemodynamic responses observed in the BOLD signal and the underlying neural activity is not fully understood. Electrophysiology, on the other hand, has a high temporal resolution and can give us better insight into the changes in neuronal activity. There are several factors involved in hemodynamic and neural activity changes, such as the type of cells generating the neural activity, the coupling between energy consumption and energy supplies to the active area and the type of neural activity itself (Logothetis, 2003). I will be focusing on the latter as it seems to highly contribute to BOLD fMRI generation.

1.6 HRF Models for fMRI Data Analysis

Analysis of fMRI data begins with understanding the relationship between the stimulus and the neural response derived by it. While the stimulus stream can be modeled as some impulse or delta functions, the neural response is assumed to be the stimulus function convolved with an HRF. The resulting time series are used as regressors in a general linear model (GLM). This is the basis of statistical parametric mapping (SPM) approach (Friston, 2003).

BOLD signal is an indirect measure of neuronal activity, but its variations do not only come from neuronal fluctuations. In fact, the variations may also arise from global magnetic susceptibilities, vascular variations in individual brain areas, the baseline cerebral blood flow and other physiological sources (Bush and Cisler, 2013; Handwerker et al., 2004).

Notwithstanding, HRF links neural responses to fMRI data and more importantly, it can adjust the variations of neural responses between different brain regions and across subject populations (Buxton et al., 2004; Handwerker et al., 2004; Kumar and Penny, 2014; Roebroeck et al., 2011). The controversy of how and in what extent the HRF variations change the results of connectivity maps was first brought up by David et al. (2008) who compared the network connectivity with and without deconvolving the BOLD signal into its basis functions. They showed that the connectivity is only accurate when deconvolution is performed.

The HRF has been investigated for both task-based fMRI and rs-fMRI and although it is more difficult for rs studies with no stimulus or task (unless relying on physiological

hypotheses) (Havlicek et al., 2011), the HRF can be modeled by explicit inputs and assumptions made based on the stimulus stream (Gonzalez-Castillo et al., 2012; Riera et al., 2004). What these studies attempted to do was to correct for inter-subject and inter-region variability of the HRF.

It was observed that there is more HRF variability in the former and one HRF model can be employed for several brain areas (Handwerker et al., 2004). Even GLM simulations demonstrated only slight improvements with subject-specific HRFs compared with canonical HRF, which is used in GLMs by default, or SPM double gamma HRF (Handwerker et al., 2004; Zumer et al., 2010). This is indeed an active area of research and there is still no solution that can solve all the problems about HRF variability and depending on the question asked in each study, it is not well understood how this variability may affect the results.

1.7 Neural Basis of BOLD fMRI

A brief overview of the different types of neurophysiological signals is described here in order to better understand the underlying neural activity of the BOLD signal. In theory, if two separate regions of a neuron have unequal membrane potential, there will be a flow of current in the neuron as well as a return current in the extracellular path (Logothetis, 2002). Observing the flow of currents from an extracellular perspective, there is this inward flow of Na^+ into the neuron (this active region is called sink) and also an outward current to inactive regions of the neuron (also called source). These currents generate extracellular field potentials (EFPs) (Hodgkin and Huxley, 1952; Logothetis, 2003). The signal that an electrode inserted in the brain records are mean EFPs (mEFP) in close

vicinity and this is because the lipid membranes act as capacitance in extracellular medium, in which neurons are embedded in.

Depending on the position of the recording electrode and its physical properties, like impedance, mEFPs reflect single unit action potentials (AP) or the totality of potentials in that region. The latter can be local field potentials (LFP) or multi-unit activity (MUA), which will be explained later.

At the microscopic level, neuronal communication is indirectly reflected in fMRI-created images. Most of the communication between neurons happens at the synapse, which is the junction where the presynaptic process of an axon is in close proximity to the postsynaptic process of a dendrite or cell body. Depending on the type of neurotransmitter (being excitatory or inhibitory) released by the presynaptic neuron, a specific channel will open to allow ion flow into or out of the cell.

If positive ions (Na^+ , Ca^{2+} , K^+) enter the cell down their concentration gradient, membrane potentials will decrease (depolarization) and an excitatory postsynaptic potential (EPSP) event will happen at the local synapse (Huettel et al., 2004). Inhibitory postsynaptic potentials (IPSP) are induced when negative ions (Cl^{-}) enter the cell or positive ions exit the cell again down their concentration gradient and increase the membrane potential (hyperpolarization). If the net depolarization at the axon hillock reaches a threshold, large numbers of voltage-gated sodium channels will open and there will be an inward flow of Na^+ via ionic channels into the neuron. The wave of depolarization, which travels down the axon, is the action potential (AP).

Since all of these diffusion processes happen along their concentration gradient, they do not need an external source of energy. But both sorts of potentials lead to changes in the ion concentration in the cell that needs energy to restore and return the cell to equilibrium. Membrane pumps such as the sodium-potassium pump, which removes three Na^+ out of the cell and brings 2 K^+ into the cell, require external energy sources. A large amount of energy in the brain is used for restoration following APs and EPSP/IPSPs (Atwell and Laughlin, 2001). This energy is supplied by aerobic and anaerobic processes beginning by glucose breakdown and the production of adenosine-triphosphate (ATP) molecules. The vascular system ensures a continuous supply of oxygen and glucose for these processes by increasing the CBF to the brain active region.

1.7.1 Single-Unit Recordings

If an electrode is placed close to the soma or axon, the measured mEFP represents the spiking rate (the number of action potentials in a second) of that neuron and the nearest neurons as well. In most experiments with single unit recording (SUR), the output of the cortical area under recording is represented by the activity of large pyramidal cells (Logothetis, 2003).

1.7.2 Multi-Unit Recordings

If the recording electrode is placed a bit farther from the spike-generating source so that APs are not dominant in the recorded signal and the electrode impedance is very low, the mEFPs reflects the total extracellular APs happening within $\sim 200 \mu\text{m}$. The magnitude of MUA is site (Buchwald and Grover, 1970) and cell-size specific (Nelson, 1966); therefore it differs in different brain regions. However, it is constant within a specific site.

When recording neuronal ensembles, MUA and LFPs are distinguished by frequency band separation. To obtain MUAs, a high-pass filter with a cutoff frequency at about 300-400 Hz is commonly used (Logothetis, 2003).

1.7.3 Local Field Potentials

The LFP is the low-frequency wave in an mEFP signal that is believed to show the superposition of synaptic currents and the total of voltage-gated membrane potentials in a local group of neurons, averaged in a volume of tissue (Mitzdorf et al., 1987). Compared to MUA, the LFP is related to the geometry of dendrites instead of cell size (Buchwald et al. 1965). In order to distinguish LFPs from recording signal, a low-pass filter with cut-off frequency of about 300 Hz is often used (Logothetis, 2003).

Fluctuations in membrane potentials reflect the input of a specific cortical area and the activity of excitatory and inhibitory interneurons (Logothetis, 2003). Phase locking of fluctuations in the membrane potential to specific frequency bands was initially under investigation in the EEG literature (Pedley and Traub, 1990). Based on correlations between certain behavioral states and the LFP observed in cortex, it can also be subdivided into different frequency ranges, such as delta (δ , 0-4 Hz), theta (θ , 4-8 Hz), alpha (α , 8-12 Hz), beta (β , 12-30 Hz), gamma low (γ_L , 30-50Hz) and gamma high (γ_H , 50-100 Hz).

These neural oscillations are temporally correlated; as an example, gamma band is known for communications in local cortical regions (Womelsdorf et al., 2007) and lower frequency bands seem to maintain synchronization between distant regions (Stein et al.,

2000). Furthermore, these temporal correlations are functionally related (Uhlhaas and Singer, 2010). Here are some of the functions for each band:

- Theta band: memory (Vertes, 2005), synaptic plasticity (Huerta and Lisman, 1993), top-down control and long-range synchronization (Stein et al., 2000).
- Alpha band: inhibition (Klimesch et al., 2007), attention (Thut et al., 2006), consciousness (Palva et al., 2005), top-down control (Stein et al., 2000), long-range synchronization (Doesburg et al., 2009).
- Beta band: sensory gating (Hong et al., 2008), motor control (Kilner et al., 2000). It also has some overlap with alpha band, such as attention (Gross et al., 2004) and long-range synchronization (Kopell et al., 1999).
- Gamma band: memory (Tallon-baudry et al., 1998), synaptic plasticity (Wespatat et al., 2004), attention (Fries et al., 2001), consciousness (Melloni et al., 2007), perception (Gray et al., 1989).

1.7.4 BOLD Signal Is A Reflection of Synaptic Activity

In order to find the contribution of each type of neural activity, there have been several studies recording LFPs, single- and/or multi-unit activity simultaneously with BOLD-fMRI responses. In 2002, Logothetis published a paper that reported recordings all three types of neural activity from monkey visual cortices and compared them with BOLD responses that were simultaneously recorded (Logothetis, 2002). His results show that despite single- and multi-unit activities that adapted a couple of seconds after the visual stimulus onset and returned to the baseline, LFPs remained correlated with the BOLD response the longest. Also, in linear system analysis, LFPs had the largest magnitude signal and this suggested that LFPs were better estimating the fMRI signal than MUAs.

This important finding regarding the neural basis of BOLD signal has been interpreted as evidence that this signal mostly reflects the incoming input and local processing in a region and not the output (Logothetis et al., 2001; Logothetis, 2003).

Meanwhile, since the fMRI signal is sluggish and does not have high temporal resolution, LFPs, which fluctuate more slowly than single- and multi-unit activities, seem to be a better candidate to be compared with BOLD-fMRI. Leopold and colleagues examined these fluctuations recorded from multiple regions in monkey visual cortices with surface multi-electrode-arrays (MEA) (Leopold et al., 2003). The experiment yielded several results: 1) the band-limited power (BLP) of LFPs fluctuated at various frequencies with maximal amplitude at very low ranges of frequency (<0.1 Hz); 2) BLP of gamma LFP showed the highest coherency between the electrode pairs; 3) in contrast to raw LFP, BLP coherency fell off more gradually as a consequence of electrode or cortical distance; 4) the coherence and shape of BLP changes were similar in two different conditions, those being at rest (monkey was inactively sitting in a dark room) and task condition (monkey was involved in a binocular rivalry task). These global coherences are thought to provide us with good information about the intrinsic activity in the resting brain and also due to the low frequency of the BLP signal, they can be a good comparison point between LFP and BOLD. Even recordings in awake monkeys have shown that BOLD responses are more prone to changes in LFPs than action potentials (Goense and Logothetis, 2008). The procedure of how BLPs were calculated from the LFP signal will be discussed in the method section.

1.7.5 How to Study Local Field Potentials

Although it was first with fMRI technique that intrinsic activities in the brain were observed to have spatiotemporal patterns, correlating patterns of neural activity can be observed in microelectrode recordings as well. One of the main features of intrinsic brain activity is the intrinsic coupling mode (ICM) (Engel et al., 2013). ICMs display high spatiotemporal patterns and can bias the cognitive processing of the brain. There are two main types of ICMs that have different dynamics, origins and functions. Phase ICMs emerge from phase coupling between band-limited signals, whereas envelope ICMs come from amplitude or power coupling between band-limited signals (Engel et al., 2013).

There are some analyses that can be applied to LFPs for studying ICMs, one of which is coherence. Coherence finds the linear relationship between oscillatory signals and, if they are aligned in their phases and are similar in amplitudes, coherence will have a high value. In case of phases being aligned, this value will indicate phase coherence or phase locking value and determines phase ICMs (Lachaux, et al., 1999). Furthermore, the signals will be correlated if there is similarity between their amplitudes or power. While phase ICMs are more meaningful in electrophysiology signals, envelope ICMs can be investigated with both electrophysiology and fMRI. In terms of their putative functions, envelope ICMs are known to control neural activation in a brain region and phase ICMs direct the flow of cognitive contents (Engel et al., 2013).

1.8 Microcircuitry Differences across the Cortex

Once it was believed that the mammalian brain has a uniform neuronal circuitry (Rockel et al., 1980) and based on extensive works done in cats and monkey visual cortex

(Douglas and Martin 2004; Gilbert, 1983) a canonical cortical microcircuitry (CCM) model was proposed. The main features of this model include ascending inputs to granular layer IV (L4) and while primary sensory areas are shown to have well-developed L4, some prefrontal areas lack this layer (Paxinos et al., 2000). For example, Brodmann area 9/46d and 46 in primates have distinguishable L4, but area 9 does not (Petrides and Pandya, 1999). Another influential example is area V1 in the occipital lobe that has a thick L4 that receives afferent inputs from the thalamus. In contrast, supplementary eye field (SEF) does not have a L4 (Brodmann, 1909).

There is growing evidence that while agranular areas share similar aspects of the CCM to granular areas, major differences are also present. Godlove and colleagues conducted LFP and spike recordings with laminar multi-electrode arrays in SEF while the monkeys were sitting in a dark room and light flashes would appear in a block design (darkness + light flash) (Godlove et al., 2014). They showed that although the pattern of synaptic current in the middle layers is similar to current source density (CSD) pattern observed in early sensory cortex (Riera et al. 2012), the current density was weaker in the SEF. Also, in contrast to CCM model, dual current sinks appeared simultaneously in layer III and V and visual response latencies did not differ across layers.

LFPs recorded from monkey SEF during resting state, also shows both similar and different aspects of CCM model compared to primary visual cortex V1 (Ninomiya et al., 2015). Here the authors showed that the coupling between gamma amplitude and alpha-beta phase in SEF was prominent only in Layer III, while the same coupling exists in layer II, III and V in V1 area.

These results conclude that correlation between BOLD and neural activity observed in different brain areas such as PFC or primary visual cortex, should be compared and interpreted with caution, considering the different underlying microcircuitry

1.9 Human and Monkey Brain Similarities

RS-fMRI animal investigations have been limited to mostly rats, macaques (an old-world monkey species) and also recently marmosets (for review see Hutchison and Everling, 2012). While the last common ancestor of humans and macaques dates back 25 million years ago, rodents and primates diverged from one another about 80 million years ago (Kumar and Hedges, 1998). Also, the amount of volume, occupied by the neocortex is 28% in rats, 72% in monkeys and 80% in humans (Passingham, 2009). Meanwhile, it has been acknowledged that macaque and human brains are highly comparable in terms of functional organization (Petrides et al., 2005; Rees et al., 2000), anatomical connections (Croxson et al., 2005) and cytoarchitecture (Petrides and Pandya, 1999).

At the same time, most of the electrophysiological recordings in humans are performed in a clinical setting. This type of surgery is limited to certain patients such as epilepsy patients and this approach adds limitations for generalizing the results to normal human brain (Ojemann et al., 2013). Comparisons between epileptic and non-epileptic cortices show different BOLD connectivity measures (Bettus et al., 2011) and changes in network connectivity (Bullmore and Sporns, 2009). For these reasons and the above-mentioned similar observations of DMN and RSNs, non-human primates are the most appropriate model for fMRI studies.

1.10 Neural Correlates of Resting-state BOLD fMRI

The best way to evaluate the neural correlates underlying rs-fMRI is to simultaneously acquire both electrophysiological and hemodynamic signals. This approach has been carried out in non-human primates and humans with various electrophysiology techniques such as EEG, ECoG, SUR, MUA and LFP recording at different brain states, including rest and anesthesia or while performing a task (See Figure 2).

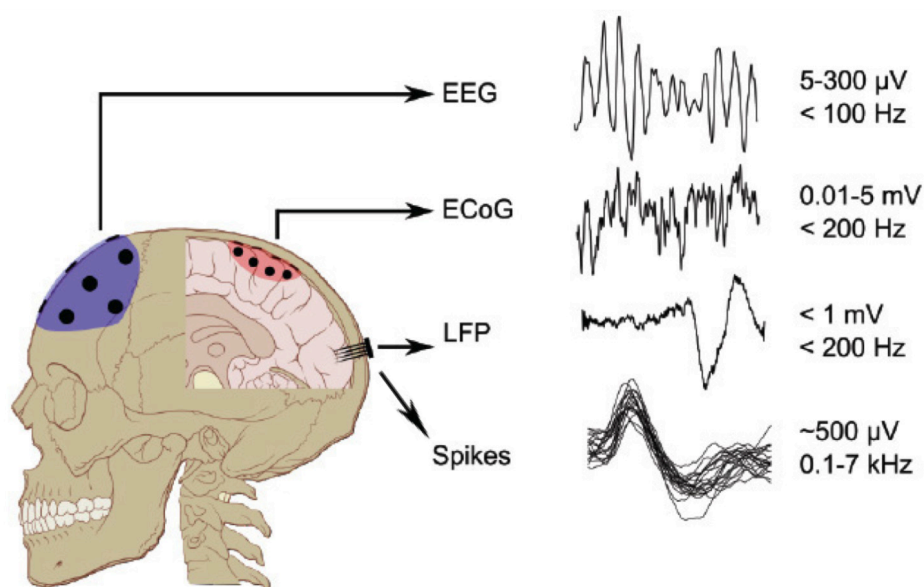


Figure 2: Recording Electrophysiological Signals With Different Techniques. EEGs are recorded from the scalp, which attenuates the signal amplitude. ECoGs are recorded from pial surface and it can be seen that the signal amplitude is larger compared to EEGs. LFPs, spikes and MUA (not shown here) all can be recorded with an inserted electrode into the cortex. Notice the high frequency of spikes. Adapted from lifesciences.ieee.org

There are many studies that support a temporal coupling between EEG and rs-fMRI signals in humans (Laufs et al., 2003; Picchioni et al., 2011) The result of simultaneous EEG-BOLD fMRI in humans engaged in a visual attention task demonstrates that there is positive correlation between high-gamma power (60-80 Hz) and BOLD fluctuations,

while this correlation is negative for alpha (~10 Hz) and beta (18-28 Hz) power (Scheeringa et al., 2011). Scheeringa et al.'s results suggest that high frequency neural oscillations and low frequency oscillations contribute to BOLD signal generation independently. Interestingly, there has been found high spatial correlation between conventional RSNs and the BOLD correlates of EEG topographies (Britz et al., 2010; Jann et al., 2010). BOLD correlates of EEG topographies were determined by convolving simultaneously recorded EEG signals with an HRF model and fitting them into a GLM.

Results from intracranial recordings of ECOG show that widespread ECOG measures exhibit correlated networks appearing between recording sites that are comparable to BOLD-fMRI correlated and anti-correlated networks (He et al., 2008; Keller et al., 2013).

While EEG and ECOG are mostly conducted in human studies, intracortical recordings (single- and multi-unit and LFP) are widely performed in animal lab studies. In a landmark study, Shmuel and Leopold (2008) conducted simultaneous fMRI and intracortical recordings from area V1 primary visual cortex in anesthetized monkeys. They found that slow fluctuations of the BOLD signal correlated highly to BLP of high gamma LFP signals and also to the spiking rate of neurons in the vicinity of the electrodes and the multi-unit activity band power changes (Shmuel and Leopold, 2008). The relationship between the single-unit activity of neurons and BOLD fMRI has been investigated in some human studies as well (for review see Ojemann et al., 2013) and while Nir and colleagues could find interhemispheric correlations between BOLD and single-unit firing rate at rest (Nir et al., 2008), Ojemann et al. (2010) did not see colocalization between unit firing and BOLD increase or decrease during silent word pairing in human subjects.

Among three types of intracortical signals, LFPs fluctuate in lower frequencies than single-unit and multi-unit activities. Thus, the fluctuations in the LFP power are most comparable to low frequency BOLD fluctuation. In one study, simultaneously electrical and hemodynamic responses recorded in cat visual cortices exhibited tight positive correlation between the power of gamma oscillations and fMRI signals and negative correlation for delta band (Niessing et al., 2005). When the visual stimulus intensity was increased, the hemodynamic response, gamma LFP oscillations and spiking activity increased as well. However, when the stimulus intensity was constant, only the changes in the power of gamma LFP and hemodynamic response were highly correlated.

The divergence between single-unit and LFP studies may arise from the fact that gamma LFPs are associated with high frequency discharges of inhibitory interneurons (Traub et al., 1996) and their synapses spread within neighboring cortical areas. These interneurons are believed to contribute to local energy consumption in the brain cortex and to be the cause of hemodynamic response (Azouz and Gray, 1999). Therefore, the link between hemodynamic responses and gamma oscillations might reflect the activity of inhibitory interneurons (Niessing et al., 2005; Nir et al., 2007).

Another study used information theory to distinguish the statistical dependency between simultaneously acquired BOLD signals and LFP bands in areas V1 and V2 of anesthetized monkeys (Magri et al., 2012). Their results showed that gamma was the most informative band, while alpha and beta power carried complementary information.

In contrast to the observed negative correlation for the delta band by Niessing et al. 2005, it has been demonstrated in awake monkeys at rest that the spontaneous hemodynamic

response is positively correlated to the power of higher gamma LFP signals (40-80 Hz) and lower frequency bands of LFPs (2-15 Hz) recorded between each volume acquisition (Schölvinck et al., 2010). The interleaved acquisition paradigm here was to avoid the neural signal being polluted by electromagnetic interference. Interestingly, the highest correlation was found when the regional cerebral blood volume (rCBV), lagged the neural signal by six to eight seconds for gamma band, while this lag did not exist for lower band.

On the other hand, simultaneous fMRI and microelectrode recording in anesthetized rats showed that time-lagged correlation between infraslow LFPs (<1 Hz) and the BOLD signal is significant (Pan et al., 2013; Thompson et al., 2014).

Bringing all these studies together, it has been well established that hemodynamics of different brain regions are highly correlated to the neural activities simultaneously recorded. While the results are not completely consistent, distinct LFP bands seem to contribute differently to hemodynamic changes in different regions of the cortex, whether positively or negatively.

Therefore, in order to further investigate the contribution of electrophysiological activity to spontaneous activity in resting-state, we still need to better explore the correlational relationship between fMRI and neural fluctuations.

1.11 Rationale and Hypothesis of the Current Study

Owing to its superior spatial resolution and whole-brain coverage, fMRI has been widely used to examine spontaneous brain activity, quantifying blood oxygenation changes that are indirectly coupled to underlying neural activity (Raichle and Mintun, 2006). Despite

great advances in understanding the neurovascular coupling mechanisms and the relationship of neural activity to changes in blood flow, blood volume and oxygen metabolism (Leopold et al., 2003), the underlying neural basis of fMRI is poorly understood. This is particularly true of spontaneous BOLD fluctuations that can reveal intrinsic functional connectivity between regions and has continued to improve our understanding of the brain's underlying physiological principles (Hutchison et al., 2012).

The purpose of this study is to gain deeper insight into the neural correlates of spontaneous BOLD-fMRI signal by simultaneously recording local field potentials in the macaque prefrontal cortex using bilaterally implanted multi-electrode laminar arrays. BLPs of LFPs have been shown to be the most related neural activities to BOLD fluctuations (Logothetis, 2002).

We first aimed to evaluate the correlation between LFPs (1-100 Hz) and rs-BOLD-fMRI signals to find the specific frequency band(s) that yields the highest correlation. We hypothesized that positively and negatively connected regions showing antagonistic relationships will exhibit spectral relationships with distinct BLPs. Second, we explored the variations of canonical hemodynamic response function in distinct cortical areas to find the optimal HRF that can best fit in a GLM and estimate the BOLD response and also increase the correlation between BLPs and BOLD signals acquired in macaques at rest.

2 Methods

All surgical and experimental procedures were carried out in accordance with the Canadian Council of Animal Care policy on the use of laboratory animals and approved by the Animal Use Subcommittee of the University of Western Ontario Council on Animal Care (see Appendix A).

2.1 Animal Implantation

Data was obtained from 2 macaque monkeys (*Macaca fascicularis*; Monkey 1: male, 9.5 kg, Monkey 2: female, 6.1 kg). Electrode implantation surgery was conducted more than 5 weeks before the first scan and the animals were bilaterally implanted with MRI-compatible 16-channel multi-electrode laminar arrays with 150 μm spacing (A1x16-5mm-150-703-MR_CM16, NeuroNexus, Ann Arbor, MI) in prefrontal cortex area 9/46d (see Figure 3).

First, a bone flap was removed in order to spot the caudal portion of the principal sulcus in the cortex and then the dura was cut to expose the cortex and locate the principal sulcus and upper arm of the arcuate sulcus. While simultaneously monitoring the electrophysiological recordings with BrainAmp MR+ amplifier and BrainVision Recorder software (Brainproducts, Gilching, Germany) to make sure about the placement of the electrode across cortical layers, the electrode was lowered mechanically and perpendicular to the cortex to avoid penetrating the white mater (WM).

The dura was drawn back and references and ground wires were placed on the dura underneath the skull. Finally, bone defect was repaired with the previously removed bone flap and gel foam. Further, an MRI-compatible custom-built acrylic head post was

implanted to allow restraint of the head during data collection. Implants were secured to the skull with 6-mm ceramic bone screws (Thomas Recording, Giessen, Germany) and dental acrylic.

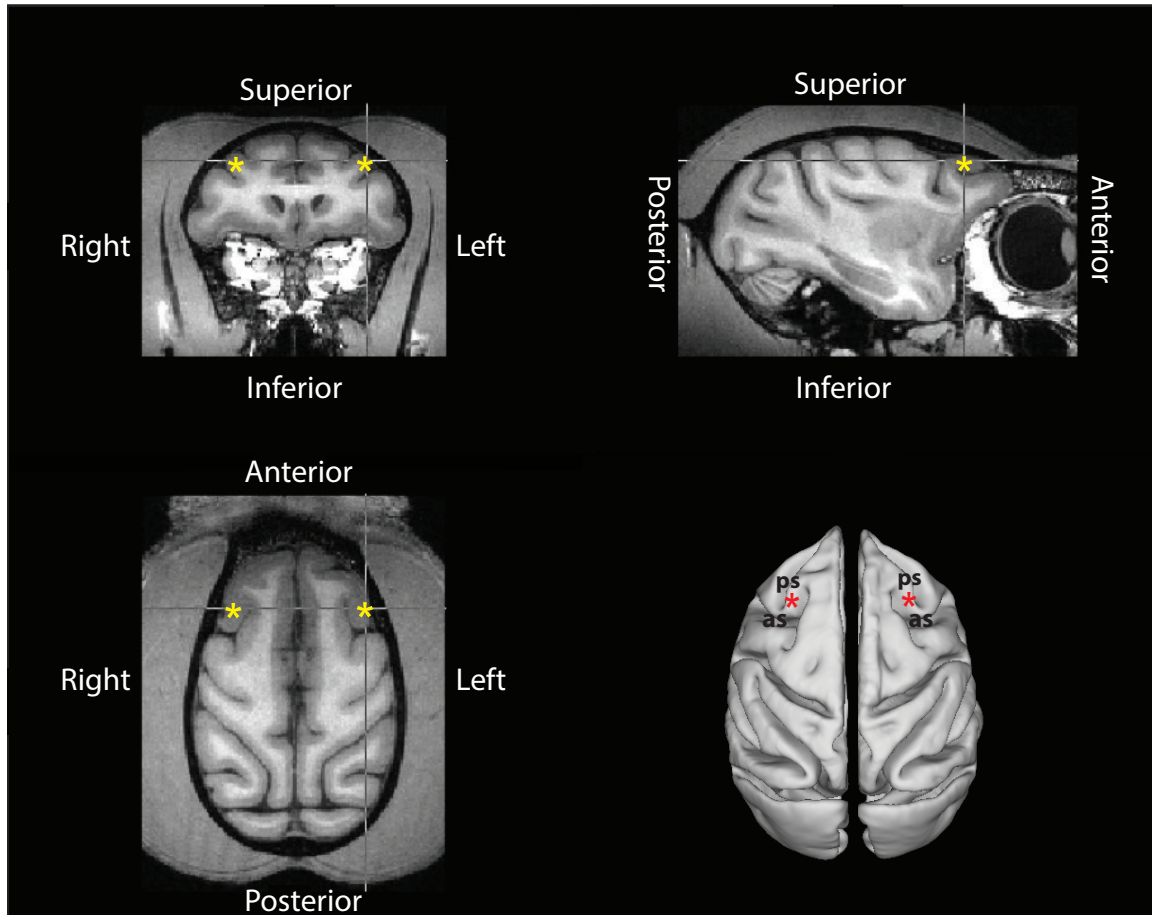


Figure 3: Electrode Placement from Different Views. Yellow asterisks on the top row and the left bottom panels show the place of the electrodes on F99 standard space and the red asterisks on bottom right panel point where the electrodes were implanted relative to principal and arcuate sulci on a surface map of the two hemispheres.

2.2 Animal Preparation

In preparation for image acquisition, monkeys were injected intramuscularly with atropine (0.5 mg/kg) and acepromazine (0.02 mg/kg) followed by intramuscular of ketamine hydrochloride (7.5 mg/kg) and medetomidine (0.0125 mg/kg) and then intravenous administration of 2.5 mg/ml of propofol via an intravenous catheter in the saphenous vein. Animals were then intubated and switched to 1.5% isoflurane mixed with oxygen.

Each monkey was then placed in a custom-built MRI-compatible primate chair with its head immobilized using the head post and a custom RF coil, and inserted into the magnet bore. At this time the isoflurane level was lowered to 1%. At the beginning of each session the image localization, shimming, test scans and anatomical acquisitions were performed which would take at least 30 min and this would let the isoflurane level and global hemodynamics stabilize. Animals were spontaneously ventilating throughout the duration of scanning. Respiration via bellows (Siemens Corp., Union, NJ), and end-tidal CO₂ via capnometer (Covidien-Nellcor, Boulder, CO), heart rate and oxygen saturation via pulse oximeter (Nonin, PureSAT, SPO₂) were continuously monitored to ensure values were within normal limits. Warmth was maintained using a heating disk (Snugglesafe, Littlehampton, West Sussex, UK) and thermal insulation.

Anesthesia was utilized in this study to eliminate motion effects, physiological stress, and training requirements. Although it has been shown that the changes in vasodilator properties (Farber et al., 1997) due to isoflurane inhalation can refine cerebrovascular activity (Vincent et al., 2007), synchronous spontaneous BOLD fluctuations have been

previously reported using isoflurane as an anesthetic in both monkeys (Vincent et al., 2007) and rats (Hutchison et al., 2010).

2.3 MRI Acquisition

Each monkey was scanned in 3 sessions and sessions were separated by more than 10 days. Data were acquired on an actively shielded whole body 7-Tesla (T) 68-cm horizontal bore scanner with a DirectDrive console (Agilent, Santa Clara, California) with a Siemens AC84 gradient subsystem (Erlangen, Germany) operating at a slew rate of 250 mT/m/s. An in-house designed and manufactured conformal 5-channel transceive primate-head RF coil was used for all experiments. Magnetic field optimization (B_0 shimming) was performed using an automated 3D mapping procedure over the specific imaging volume of interest.

Each functional run consisted of 150 continuous echo-planar imaging (EPI) functional volumes (single shot, TR = 2000 ms; TE = 18 ms; flip angle = 60° ; slices = 40; matrix = 96×96 ; FOV = 96×96 mm; acquisition voxel size = 1 mm^3). Acquisition time of each scan was 5 min and the number of runs ranged between 12 and 15 per session. EPI images were acquired with GRAPPA at an acceleration factor of 2. Every image was corrected for physiological fluctuations using navigator echo correction. A high-resolution gradient-echo T2 anatomical image was acquired along the same orientation as the functional images (TR = 1100 ms, TE = 8 ms, matrix = 256×256 , FOV = 96×96 mm, acquisition voxel size = $375 \mu\text{m} \times 375 \mu\text{m} \times 1000 \mu\text{m}$). T1-weighted MP2RAGE anatomical images (TE = 2.5 ms, TR = 6250 ms, TI₁ = 900 ms, TI₂ = 2750 ms, FOV = 128×128 mm, acquisition voxel size = $750 \mu\text{m}^3$) were also acquired and averaged. The MP2RAGE sequence is a novel sequence found to improve noise propagation

characteristics and optimize image contrast for human brain tissues at 3-T and 7-T (Marques et al., 2010).

2.4 LFP Acquisition

LFPs were recorded simultaneously during fMRI acquisition using a BrainAmp MR+ amplifier and BrainVision Recorder software (Brainproducts, Gilching, Germany). Figure 4 shows the hardware and connections setup. Beside BrainAmp MR+, the setup includes a Synbox, Synbox Scanner Interface and a BrainAmp USB Adaptor. Synbox and Synbox Scanner Interface devices keep the MR gradient system and the amplifier clocks synchronized by detecting the clock input from the scanner and downsample it to 5000Hz. They also avoid the clock signal from scanner master clock output to be affected by MR artifacts or the distance between scanner electronics cabinet and the console. BrainAmp USB Adaptor includes all the clock circuitry to align the amplifier with the downsampled clock signal. Fiber optic cables prevent the setup getting involved in any electronic interference from the scanner.

LFP signals were sampled at 5 kHz, band-pass filtered between 0.1 and 250 Hz. Each run consisted of one-minute baseline LFP recording before the scanning was started, five-minute simultaneous LFP-fMRI recording and again one-minute LFP recording. LFPs recorded during scanning were contaminated with MRI gradient change artifact. This artifact was removed by applying an offline correction technique that is based on the average artifact subtraction (AAS) method (Figure 5) (Allen et al., 1998) as implemented in Vision Analyzer2 (Brain Products, Germany).

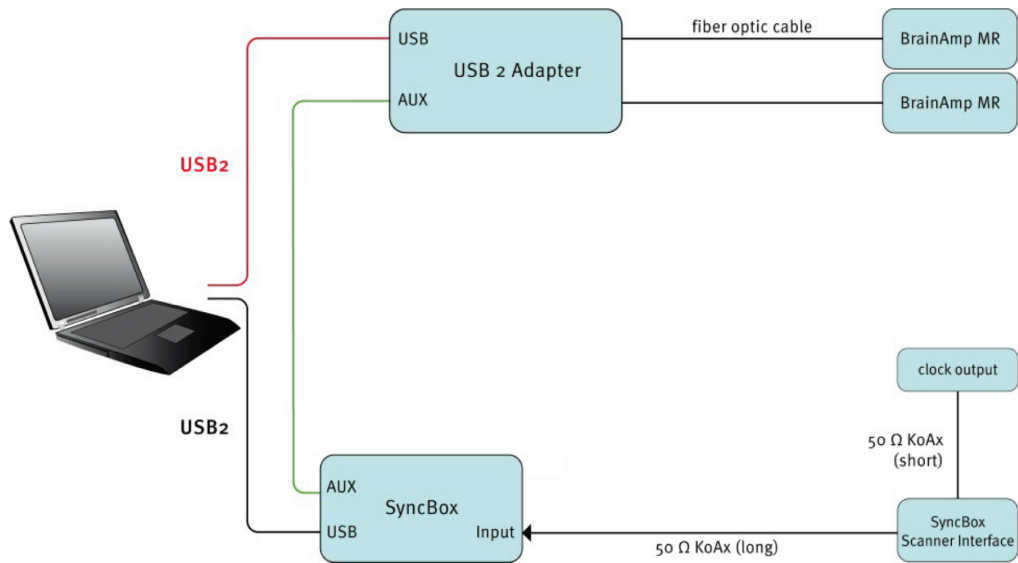


Figure 4: Hardware and Connection setup. Wiring diagram of hardware based LFP/EEG synchronization using the Syncbox is shown in this figure. USB2 connection (black) is used to program the Syncbox with any particular scanner clock frequency and the output clock signal is transferred to USB2 Adapter via Aux cable (green).

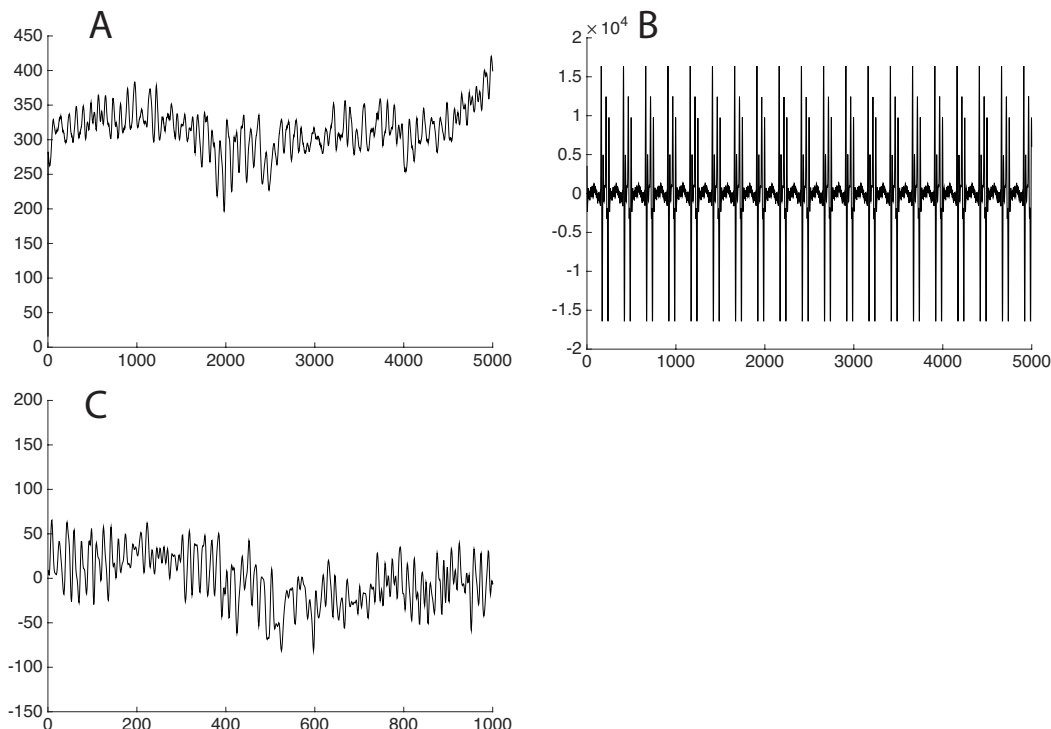


Figure 5: LFP Signal Representation During 1s Scanning. A) LFPs before starting the scanning with SR= 5KHz. B) LFPs during scanning with large artifacts with SR=5KHz. C) LFPs cleaned by AAS technique downsampled to 1KHz. Notice the amplitude change of the LFPs after removing the artifacts.

2.5 Image Preprocessing

Functional image preprocessing was implemented in the FMRIB Software Library toolbox (FSL; <http://www.fmrib.ox.ac.uk>). Preprocessing steps included motion correction (six-parameter affine transformation), brain extraction, spatial smoothing (Gaussian kernel of full-width at half maximum 3 mm applied to each volume separately), high-pass temporal filtering (Gaussian-weighted least-squares straight line fitting with $\sigma = 100$ s), and low-pass temporal filtering (half-width at half maximum = 2.8 s, Gaussian filter). Functional EPI images were nonlinearly registered to the T2

anatomical image (FNIRT; <http://www.fmrib.ox.ac.uk/fsl/fslwiki/FNIRT>), and then registered to the T1 anatomical image (six degrees-of-freedom [DOF] rigid transformation). Finally, they were normalized (12 DOF linear affine transformation) to the F99 atlas template (Van Essen, 2004); see <http://sumsdb.wustl.edu/sums/macaque/more.do>). No lag correction for the interleaved slice order was used, as the full width at half maximum of the autocorrelation function for a time series was ~ 12 s suggesting that errors in lags brought about by slice order differences in the 2 s TR period are minimal.

2.6 BOLD-fMRI Analysis

BOLD fMRI data were preprocessed using standard resting-state analysis techniques without global signal regression (GSR), which is a preprocessing step that has been observed to artificially introduce or enhance negative correlations (Murphy et al., 2009). Spherical regions-of-interest (ROIs) were manually selected in close proximity to the electrodes within area 9/46d of the prefrontal cortex and in selected areas such as the frontal eye field (FEF) and the medial parietal area 7m.

Since primates are social animals, they are being housed together with a cage mate in cases where they get along with each other. In Monkey 2, the electrode connectors had to be replaced before the first scan because the animal's cage mate damaged the connectors and the new connectors turned out to be not fully MR-compatible. Therefore, the electrode connectors caused only small local MR artifacts, which kept us from selecting seeds in the vicinity of the electrodes in area 9/46d (see Figure 6). Fortunately, for Monkey 1 we did not have such a problem and both anatomical and functional images did not show any considerable distortions or artifacts in the vicinity of electrodes.

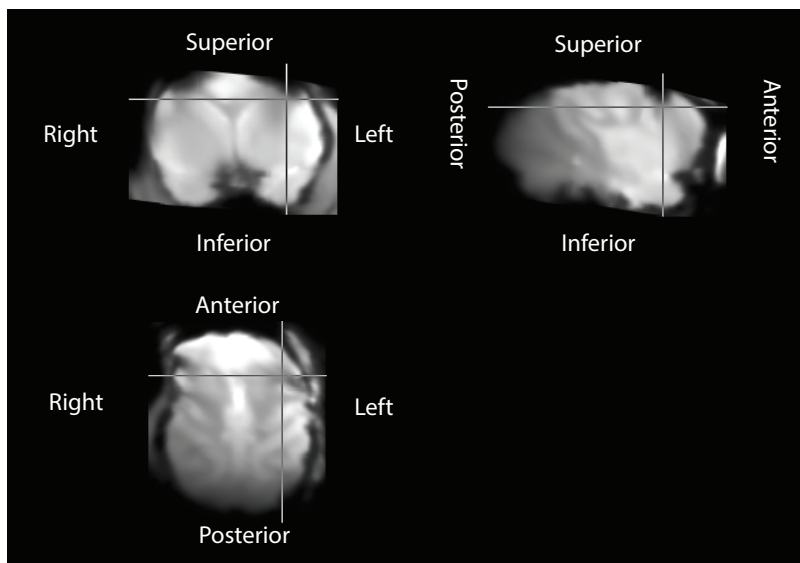


Figure 6: Functional Images of Monkey 2 overlaid on F99 Template. The cross lines shows the place of the electrode and artifacts from the fixed connectors limiting us from selecting seed regions in the vicinity of the electrodes.

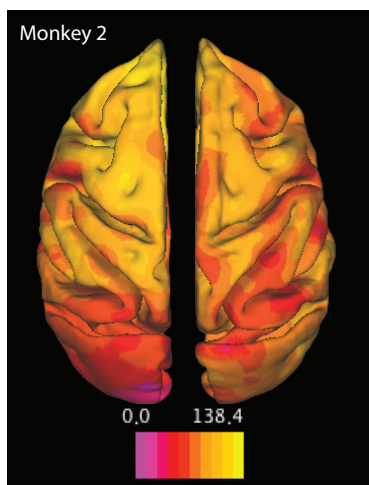


Figure 7: Signal-to-Noise Ratio Map of Monkey 2. The average signal of each run was divided by standard deviation of each voxel. Then the SNR was averaged between all the runs. It can be seen that the SNR was lower close to the electrode tip and in the occipital lobe where the head coil's profile was not homogeneous.

The mean time course for each ROI was extracted for every scan of each animal and the extracted time courses were then used as predictors in a model for multiple regressions at

the individual scan level in which nuisance covariates for WM and cerebral spinal fluid (CSF) were included. Additional covariates for motion correction (MC) were included at first and after running the analyses with and without these covariates, no significant difference was observed in the results. This would be due to the fact that the animals were anesthetized and their head and cables were completely fixed in the scanner bore. Therefore, further analyses were carried out without adding MC covariates to the GLM model.

After the first level analysis, a second level fixed-effects analysis was conducted to calculate the significantly connected voxels shared between the runs. Corrections for multiple comparisons were implemented at the cluster level with Gaussian random field theory ($z > 2.3$; cluster significance: $p < 0.05$, corrected). The thresholded z-statistic maps representing brain regions significantly correlated with each seed region were then projected from volume data to the F99 cortical surface with the CARET (<http://www.nitrc.org/projects/caret>) enclosed-voxel method (Van Essen et al., 2001).

2.7 LFP Analysis

Offline MRI artifact correction was performed based on the AAS method (Allen et al., 1998) as implemented in Vision Analyzer2 (Brain Products, Germany). By looking at the power spectrum of each LFP trace, we confirmed how clean the LFPs were from the artifacts. Only two sessions from Monkey 1 and some individual runs from Monkey 2 had to be discarded due to problems with gradient artifact removal in the LFP recordings.

After downsampling to 1000 Hz, BLP time series were computed (see Figure 8) by band-pass filtering the signal of each contact electrode in successive frequency bands (1:100, in

5 Hz steps), rectifying the signal, and resampling it every 2 s (by averaging the BLP in the TR interval which was 2s).

The BLP time series were convolved with a standard double-gamma HRF to account for the hemodynamic lag. The HRF was obtained from the SPM analysis package (http://en.wikibooks.org/w/index.php?title=SPM/Haemodynamic_Response_Function&oldid=2528715). This function has seven parameters (p) that could be manipulated with in order to explore the variations of canonical HRF to optimize the function. These Parameters were as follow:

p(1): delay of response or peak (relative to onset). Default is 6 s.

p(2): delay of undershoot (relative to onset). Default is 16 s.

p(3): dispersion of response or peak. Default is 1 s.

p(4): dispersion of undershoot. Default is 1 s.

p(5): ratio of response or peak to undershoot. Default is 6.

p(6): onset (seconds). Default is 0 s.

p(7): length of kernel (seconds). Default is 32 s.

Correlations of convolved BLP were evaluated. In a two-directional analysis, each of the BLP was used in a regression model for FC analysis as described above for the seed regions to derive voxel wise connectivity maps at the specific band. In the other direction, average network time series (across all significant [$z > 6$ and $z < -3$] regions from the seed-analysis) were calculated and then correlated with each BLP time series.

In order to find the optimal HRF, an automatic optimization approach was also used here. While in the first approach only one parameter varied and all the other parameters were held constant at their default values, in the second approach multiple parameters could be varied. Based on least mean square, the parameters were optimized to get the best fit of BLP and BOLD signals.

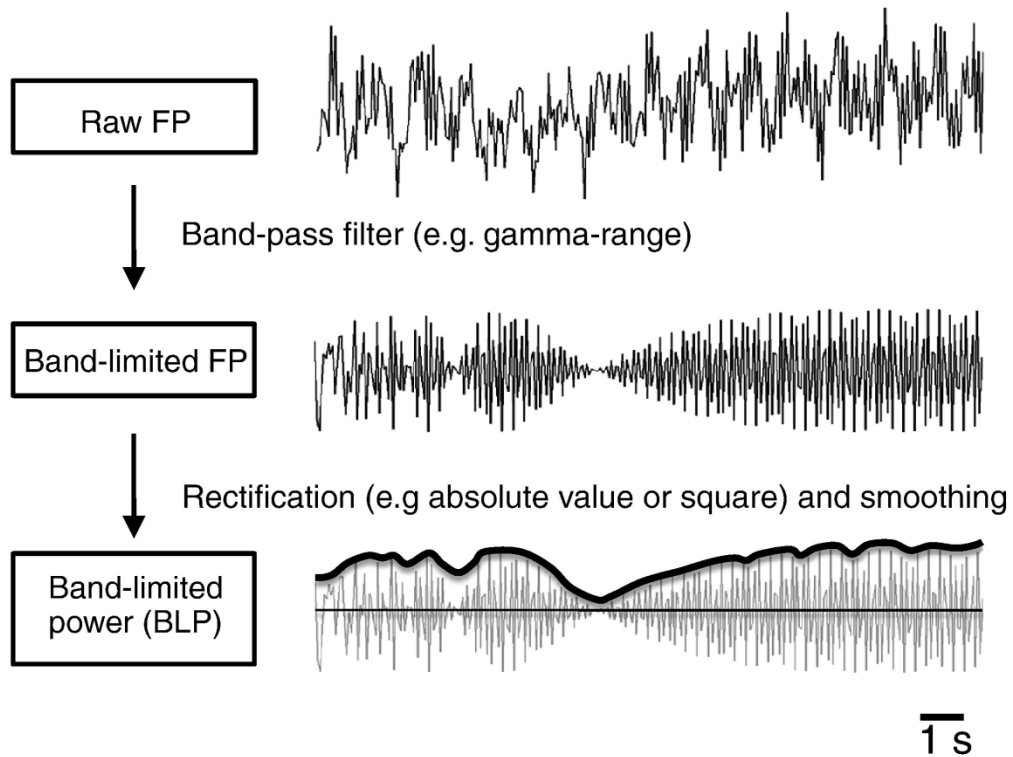


Figure 8: LFP Analysis Pipeline. The raw LFP voltage trace is first filtered into a given frequency range using a band-pass filter and then is rectified by one of a number of methods (e.g. estimating the signal envelope or squaring the band limited signal). Finally this signal is temporally smoothed and the resulting BLP signal is an estimate of the time-varying signal magnitude or signal power. Adapted from Leopold and Maier (2012).

3 Results

3.1 BOLD Seed-Based Analysis

Seed-based analysis of the BOLD signal in area 9/46d of each monkey where the electrodes were implanted (irrespective of hemisphere) showed strong, bilateral, and distributed positive FC with areas within and around the principal sulcus, medial and lateral parietal lobe including the posterior cingulate, retrosplenial cortex, intraparietal sulcus, and areas in the superior temporal sulcus (Figure 9). Similar patterns were observed in earlier work from our lab in a larger sample of monkeys (caudal cluster in (Hutchison and Everling, 2013)). These patterns were consistent with the results from tract-tracing studies (Petrides and Pandya, 1999). Anti-correlations were found among the insula, regions within the cingulate sulcus, and sub-genua cortical areas (32, 32/25) that resembled the patterns for functional division of the PFC (lateral cluster in (Hutchison and Everling, 2013)) and subgenua division of the anterior cingulate (limbic cluster in (Hutchison and Everling, 2014)). Some of these anti-correlated areas (insula, cingulate area 32) are also monosynaptically connected with area 9/46d (Petrides and Pandya, 1999).

As mentioned earlier, due to the artifact from the connectors in Monkey 2, BOLD connectivity maps could not be derived directly for area 9/46d from this animal.

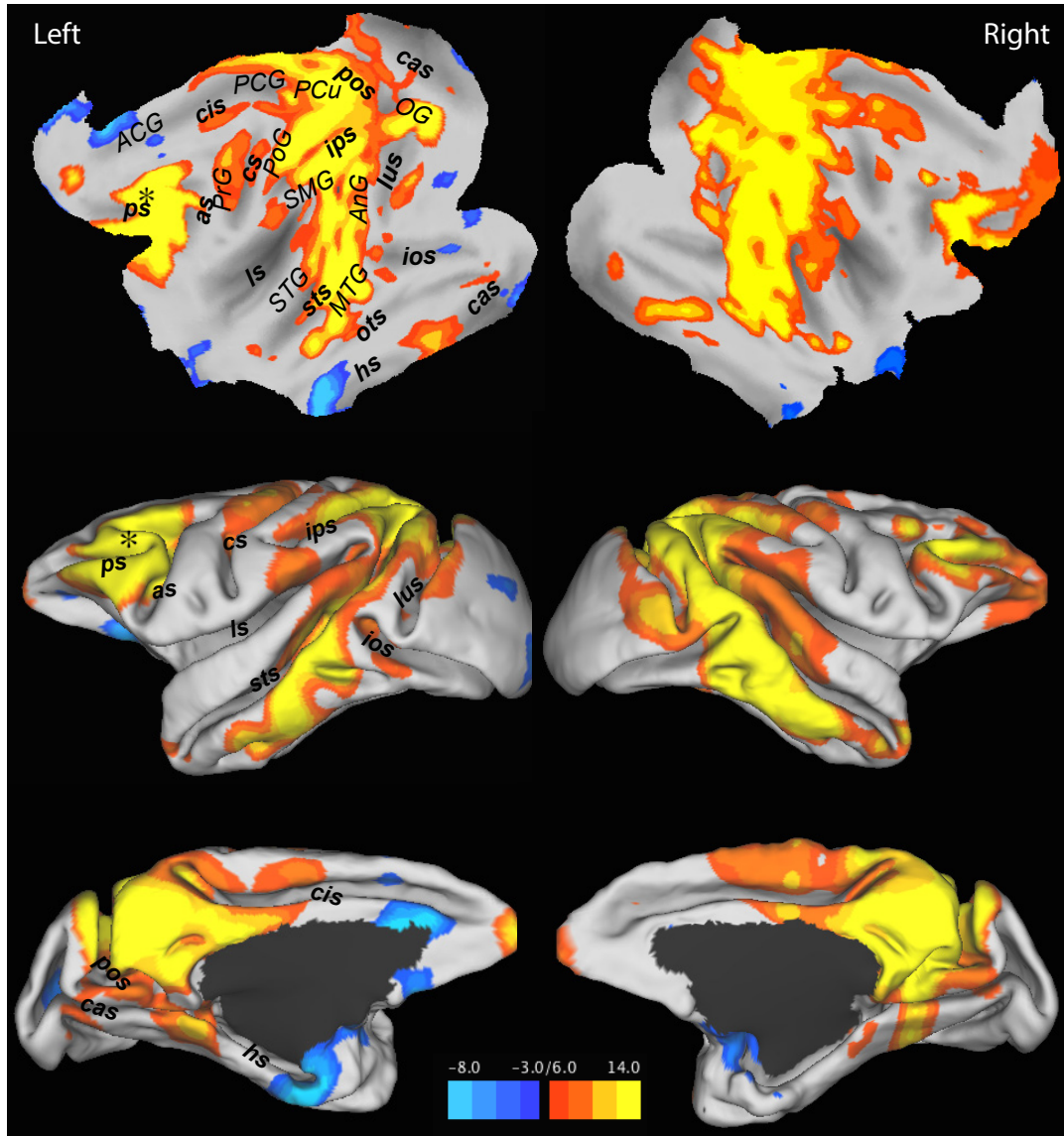


Figure 9: Spontaneous BOLD connectivity networks of Monkey 1. The map is derived from a seed region (asterisk) placed in immediate vicinity of electrode implanted in the left hemisphere. The top row represents the flattened cortical hemispheres overlaid with thresholded z-score maps ($z > 6$ and $z < -3$ cluster significance: $p < 0.05$, corrected) normalized to the space of the F99 template. The middle and bottom panels are surface maps with the same threshold. as, arcuate sulcus; cas, calcarine sulcus; cis, cingulate sulcus; cs, central sulcus; hs, hippocampal sulcus; ifs, inferior frontal sulcus; ios, inferior occipital sulcus; ips, intraparietal sulcus; ls, lateral sulcus; lus, lunate sulcus; mfs, middle frontal sulcus; pocs, posterior central sulcus; pos, parieto-occipital sulcus; prcs, precentral sulcus; ps, principal sulcus; sfs, superior frontal sulcus; sts, superior temporal sulcus.

3.2 LFP-BOLD Correlation

3.2.1 LFP-BOLD Correlation within Averaged BOLD Networks

To find the correlation between BOLD network time series and BLP bands convolved with the double gamma HRF, we averaged the BOLD activity for those areas in the positive BOLD network (yellow-red areas) and those in negative or anti-correlated BOLD networks (blue-light blue areas). For Monkey 2, we used the same indices of voxels within the positive and negative networks observed in Monkey 1. Between the averaged positive BOLD network time series and each of the BLP bins (Figure 10, red), there was a broad positive correlation with higher frequency ranges and a negative relationship with the lower frequencies. The averaged negative BOLD network time series were positively correlated with the lower BLP bins (Figure 8, blue) and negatively correlated with the higher bins in both monkeys. This relationship was also analyzed when individual seeds were used as opposed to the average network pattern, which will be explained in the next section.

Compared to previous studies where the correlation between the neural and BOLD signals were in the range of 0.2 and above (Schölvinck et al., 2010; Shmuel and Leopold, 2008), here we observed correlation as high as 0.4 and above for higher frequency bands and 0.2 for lower frequency bands.

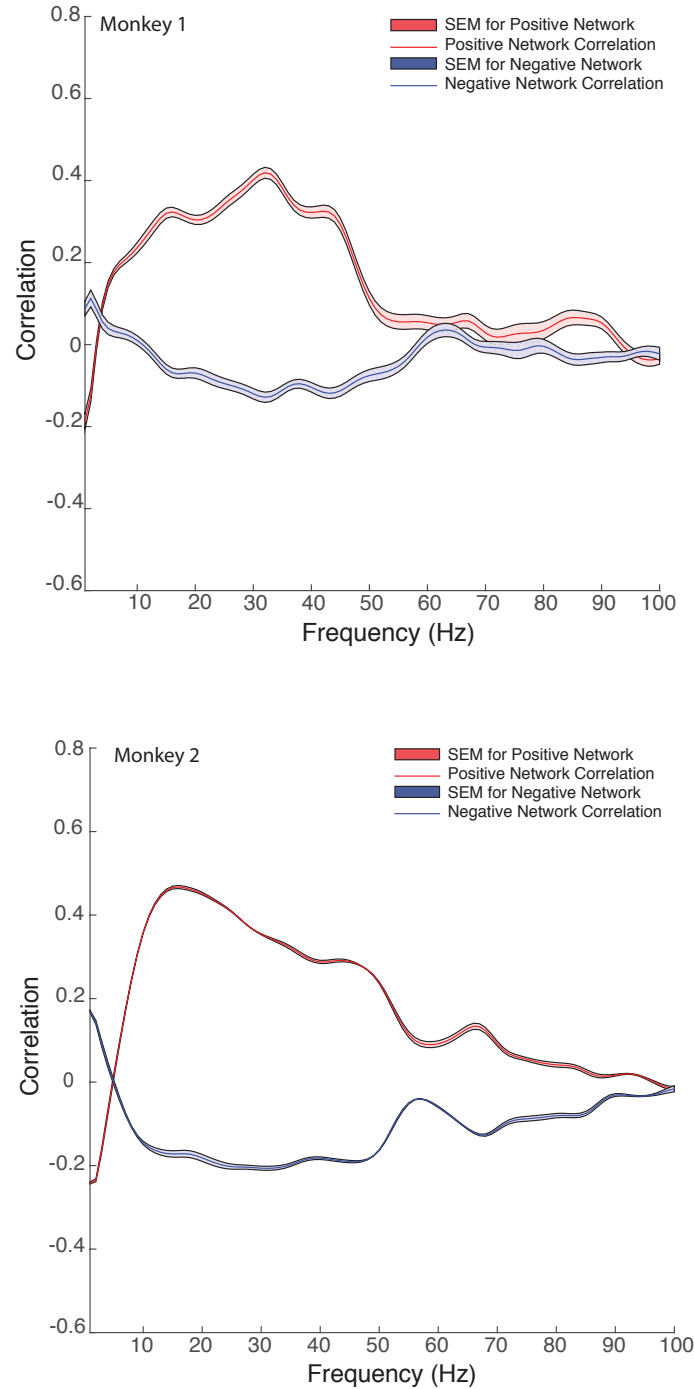


Figure 10: Correlation of BLP 5Hz bins with Average BOLD Network Time Series.

This correlation for positive (red) and negative (blue) BOLD network time series is shown for Monkey 1 on the top and Monkey 2 on the bottom panel. Time series from averaged positive networks are negatively correlated with lower frequencies and positively correlated with higher frequencies. This is opposite for averaged anti-correlated networks.

The relationship between positive or negative BOLD networks and the BLP bands was conducted for each of the electrodes in Monkey 2. Binned BLP time series showed similar relationship with the extracted BOLD signal across the 150 μm spaced contacts, (Figure 11). On Monkey 1 we could only analyze the LFP data from one channel. This could have been due to misplacement of the electrode during the implantation procedure or movement of the electrode relative to the brain over time. Further analyses were carried out using one electrode on Monkey 1 and the electrode with the highest signal power from Monkey 2.

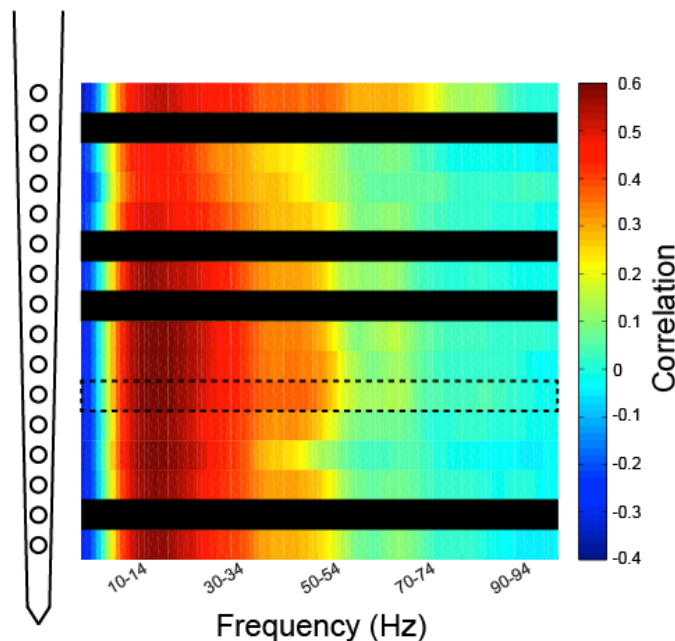


Figure 11: BLP-LFP BOLD Correlation of Contact Electrodes on Monkey 2.

Correlation of convolved BLP frequency bins with the averaged positive BOLD network time series for 16 contacts of the intracortical electrode on left hemisphere of Monkey 2 is shown here. The hatched line indicates the channel used for subsequent analysis. Blacked out rows indicate channels in which signals were not reliably recorded.

3.2.2 LFP-BOLD Correlation within Individual ROIs

We followed the same procedure here except that this time the BOLD time series were extracted from specific ROIs such as the frontal eye field (FEF) in PFC and Brodmann area 7m in the parietal cortex. These two areas are within the positive BOLD network derived from the seed-based analysis map. Therefore, we expected to see a correlation pattern similar to that of the averaged positive BOLD network correlation. Figure 12 shows the correlation of BLP bins with the BOLD time series of the positively connected FEF and 7m on ipsilateral (pink) and contralateral (black) hemispheres, relative to the electrode location in the left hemisphere.

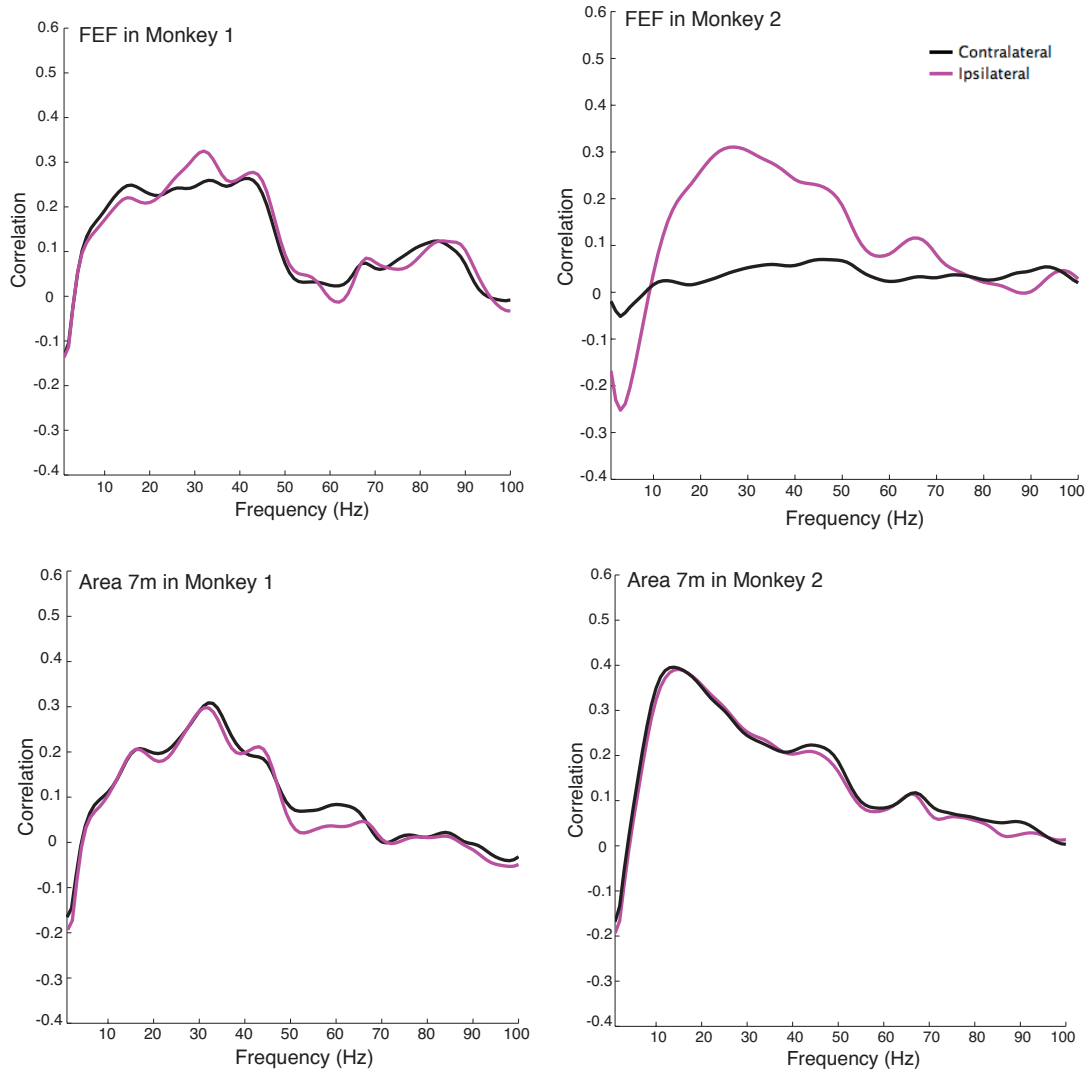


Figure 12: Convolved BLP-LFP BOLD Correlation at FEF and Area 7m. The correlation here is shown for BLP-LFP from the left hemisphere of each monkey and the BOLD signal from two brain areas (FEF and 7m). Pink traces show the correlation for ipsilateral (left) and black traces represent the correlation (right) for contralateral hemisphere. It can be seen that due to artifacts, the correlation at FEF on Monkey 2 is lower compared to Monkey 1.

As shown in Figure 12, the same correlation pattern among the averaged time series of areas in the positive BOLD networks is observed in individual ROIs. This pattern is consistent for the contralateral hemisphere as well. Due to a poor signal in the vicinity of the electrode in Monkey 2 and a small distortion caused by the electrode in Monkey 1,

the correlation is not high for the FEF area. But for area 7m, which is farther from the electrode position, there is high consistent correlation for both monkeys.

3.3 Effect of HRF Variation on LFP-BOLD Correlation

As mentioned in Chapter 2, for the correlation analyses the BLP time series were convolved with a standard double-gamma HRF to account for the hemodynamic lag. This function has seven parameters ($p(1)$ - $p(7)$), each of which was varied across 10 different values, while the other parameters held constant at their default values. First we investigated the effect of HRF parameters on the correlation between average positive BOLD network and BLP time series for both monkeys (Figure 13 and Figure 14). For each parameter, we sought the optimum HRF where we could have the highest correlation. The values ranged from below and above the default value.

The first parameter $p(1)$ varied from 1 to 10 seconds which is the delay of the HRF peak. While the correlation was increasing from $p(1)=1$ to 6 seconds, the maximum correlation was observed at 6 s and after that it began to decrease. For $p(2)$ which is the delay of the undershoot phase, the correlation did not change as the values changed. The dispersion of HRF peak which is $p(3)$ could not go beyond 7 seconds (resulted in not-a-number (NAN) values) and the highest correlation happened at 1 s. $P(4)$ is the dispersion of the undershoot and changing it had no effect on the correlation. In $p(5)$ the higher peak-to-undershoot ratio resulted in a higher correlation. However, it would reach a plateau after 6. The onset was varied by changing $p(6)$ from 0 to 9 seconds and 0 led to the highest correlation. The last parameter, $p(7)$, did not change the correlation in any direction.

A similar pattern was observed in monkey 2 (Figure 14). We also investigated the effect of HRF variation on individual ROIs such as FEF and 7m (See Figure 15 and 16) and found the results to be consistent with the previous findings. Based on these results the optimum HRF was where $p=[6\ 16\ 1\ 1\ 6\ 0\ 32]$.

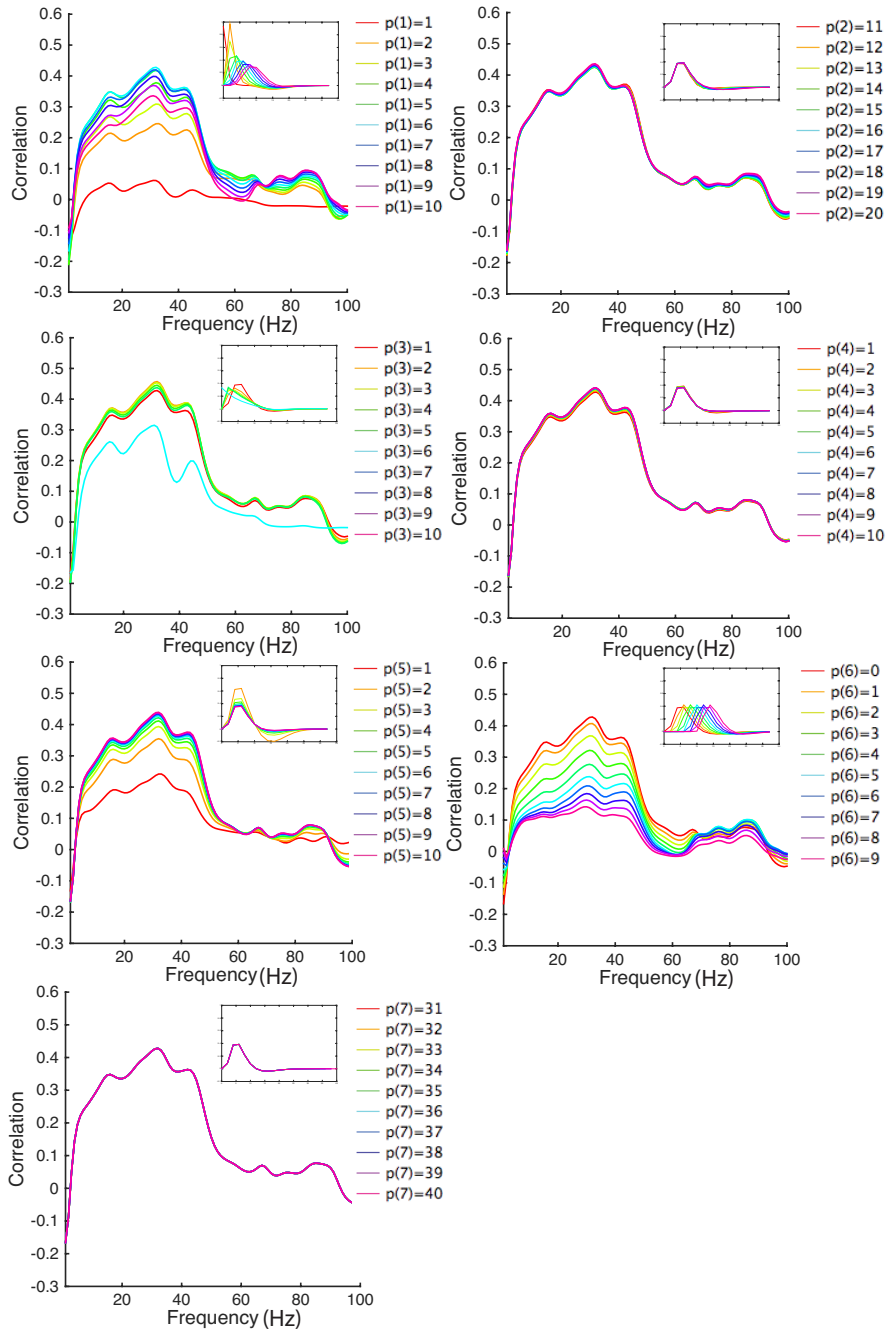


Figure 13: Effect of HRF Variation on LFP-BOLD Correlation for Averaged Positive BOLD Networks in Monkey 1. The correlation of BLP 5 Hz bins with averaged positive network time series is shown as seven parameters of HRF were individually modified for ten different values while the other parameters were held constant at the defaults. The default values are $p(1)=6$, $p(2)=16$, $p(3)=1$, $p(4)=1$, $p(5)=6$, $p(6)=0$, $p(7)=32$. The color bar beside each figure represents the parameter being modified and its ten different values for each color-coded line graph. The insets show how HRF looks like at each parameter changing for 10 values.

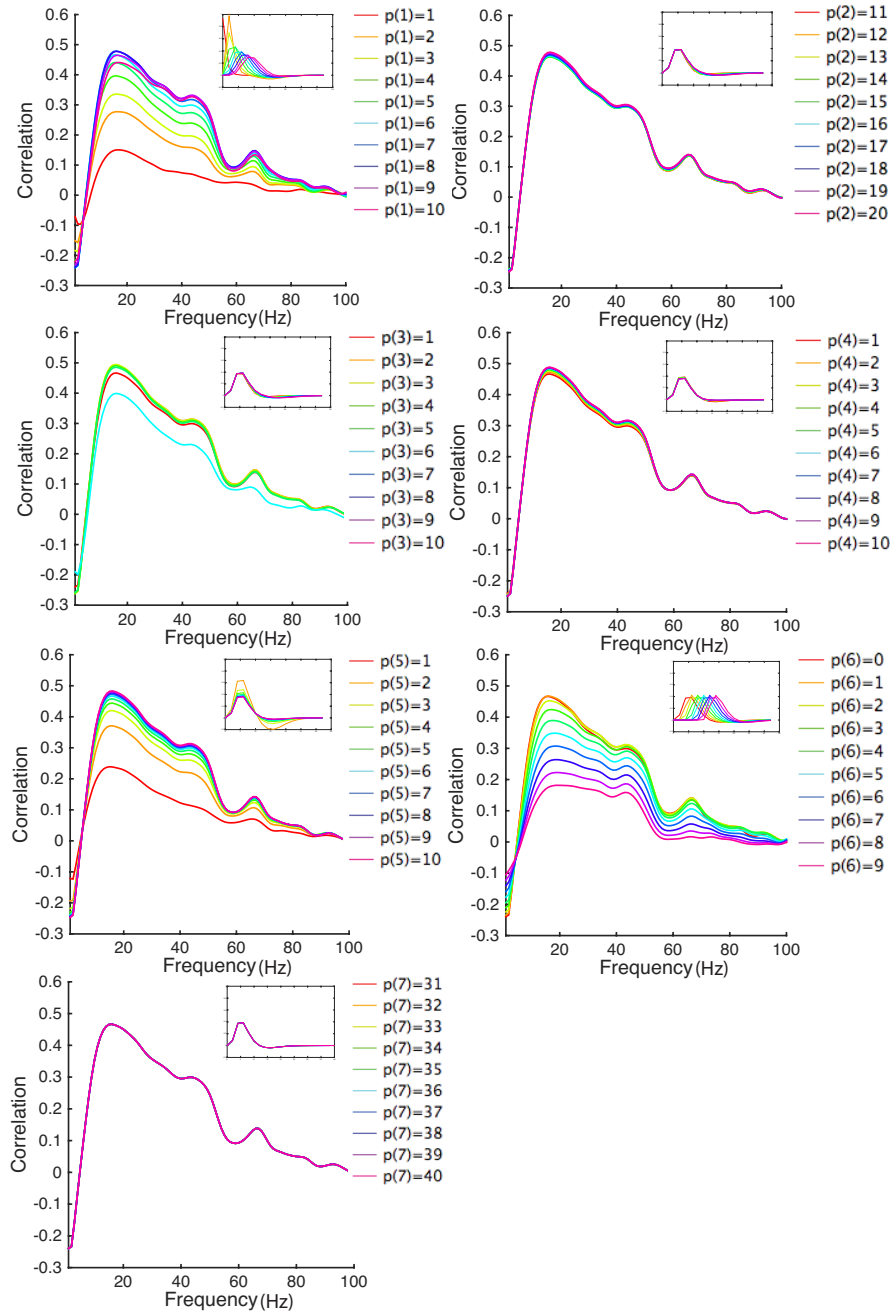


Figure 14: Effect of HRF Variation on LFP-BOLD Correlation for Averaged Positive BOLD Networks in Monkey 2. The correlation of BLP 5 Hz bins with averaged positive network time series is shown as seven parameters of HRF were individually modified for ten different values while the other parameters were held constant at the defaults. The default values are $p(1)=6$, $p(2)=16$, $p(3)=1$, $p(4)=1$, $p(5)=6$, $p(6)=0$, $p(7)=32$. The color bar beside each figure represents the parameter being modified and its ten different values for each color-coded line graph. The insets show how HRF looks like at each parameter changing for 10 values.

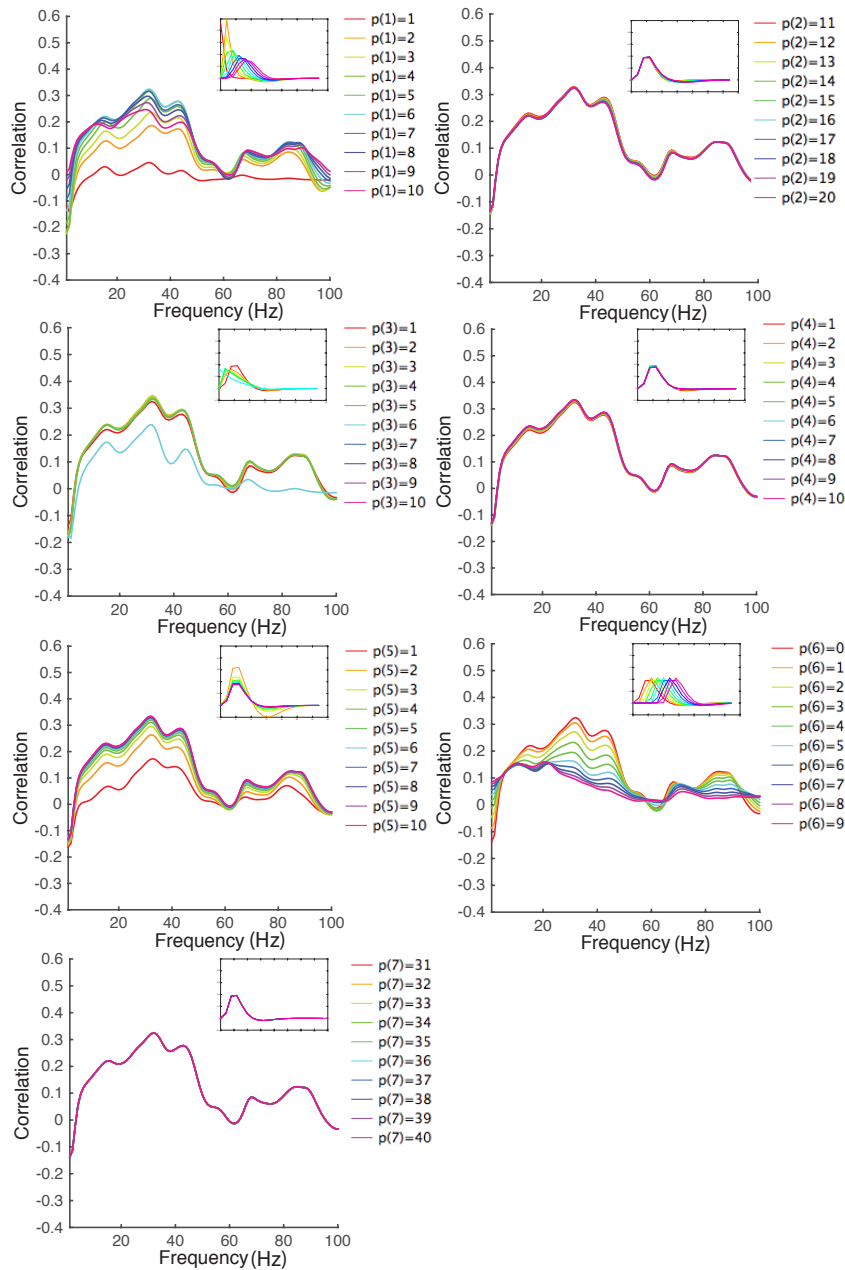


Figure 15: Effect of HRF Variation on LFP-BOLD Correlation for FEF area in Monkey 1. The correlation of BLP 5 Hz bins with averaged positive network time series is shown as seven parameters of HRF were individually modified for ten different values while the other parameters were held constant at the defaults. The default values are $p(1)=6$, $p(2)=16$, $p(3)=1$, $p(4)=1$, $p(5)=6$, $p(6)=0$, $p(7)=32$. The color bar beside each figure represents the parameter being modified and its ten different values for each color-coded line graph. The insets show how HRF looks like at each parameter changing for 10 values.

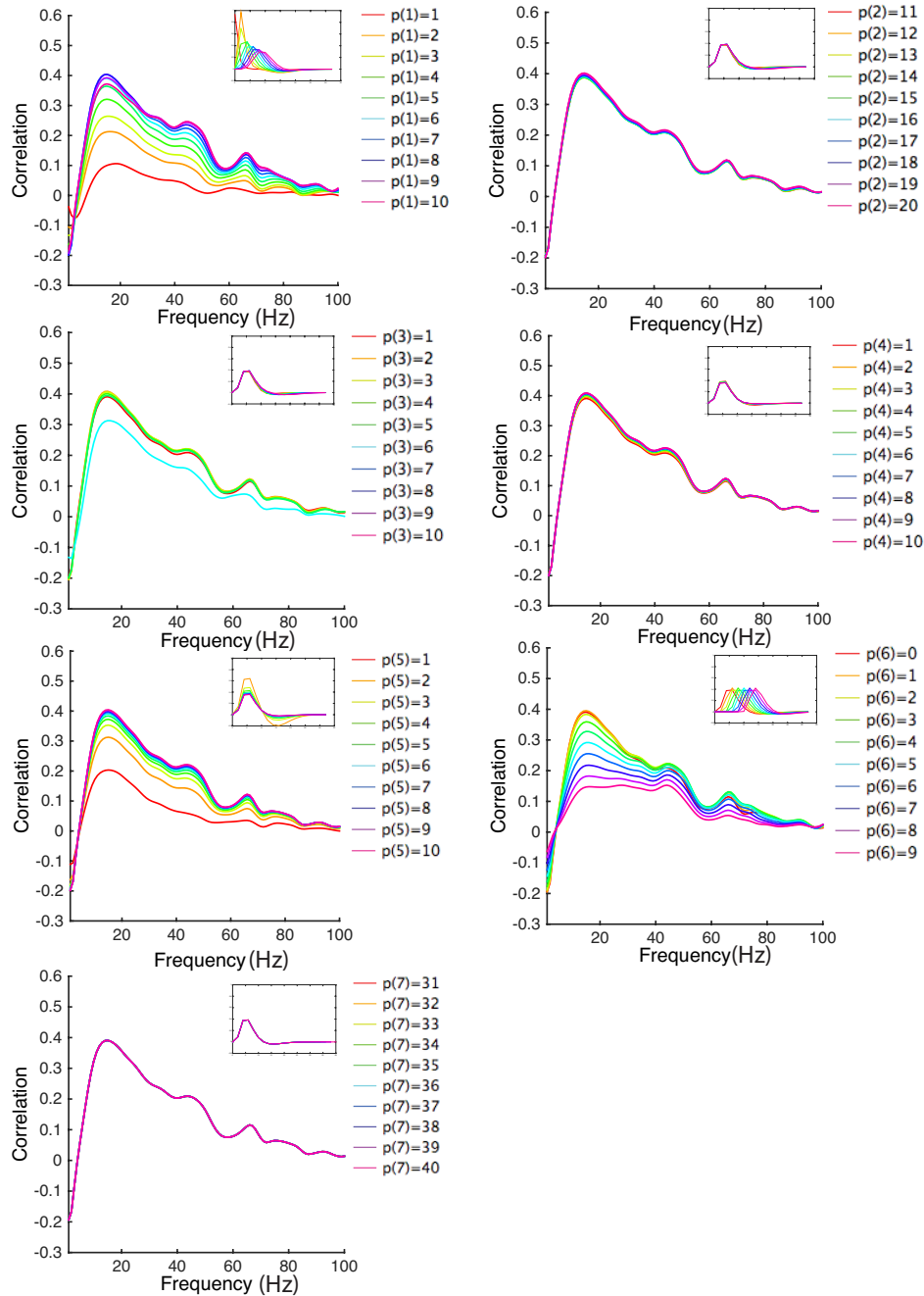


Figure 16: Effect of HRF Variation on LFP-BOLD Correlation for area 7m in Monkey 2. The correlation of BLP 5 Hz bins with averaged positive network time series is shown as seven parameters of HRF were individually modified for ten different values while the other parameters were held constant at the defaults. The default values are $p(1)=6$, $p(2)=16$, $p(3)=1$, $p(4)=1$, $p(5)=6$, $p(6)=0$, $p(7)=32$. The color bar beside each figure represents the parameter being modified and its ten different values for each color-coded line graph. The insets show how HRF looks like at each parameter changing for 10 values.

In the analysis described above, only one parameter was varied at a time while all the other parameters were held at their default values. We also took another approach and analyzed the data with an optimization technique, where multiple parameters could be changed together. Based on least mean square, the parameters were optimized to get the best fit of BLP and BOLD signals. Since the relationship between the HRF parameters is mathematically complex, this multidimensional optimization analysis allowed us to investigate the relationship between related parameters such as delay and dispersion of the peak and their effect on the LFP-BOLD correlation (Figure 17).

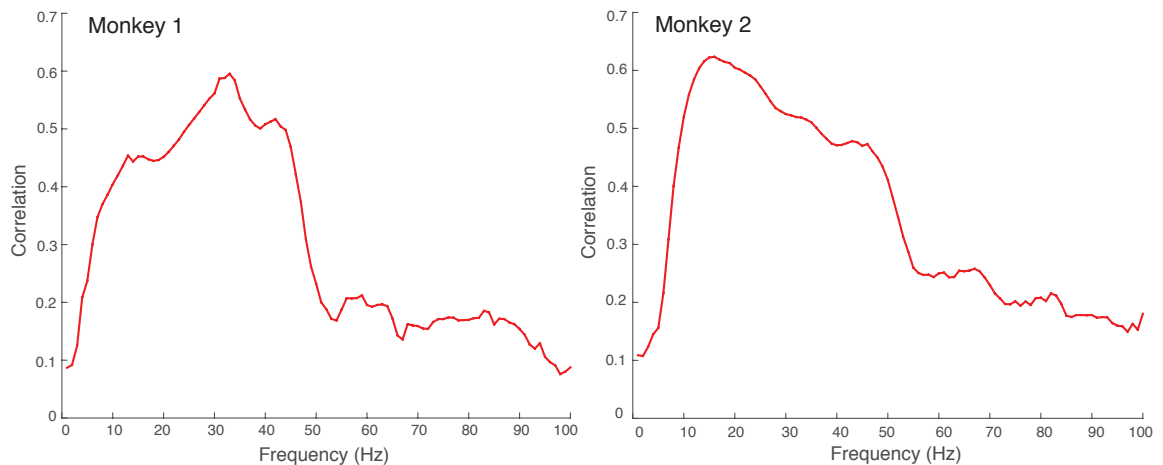


Figure 17: Effect of Automatic HRF Variation on LFP-BOLD Correlation for Averaged Positive BOLD Networks in Both Monkeys. The correlation of BLP 5 Hz bins with averaged positive network time series is shown as two parameters of HRF (delay and dispersion of the peak) were automatically changing to obtain the best fit between the BOLD and LFP time series. The optimized parameter values are shown in the next figure.

Figure 18 represents the values of both delay and dispersion of the peak for each frequency bands. The results show fluctuations for Monkey 1 and this could be attributable to the residual noise on the LFPs. Meanwhile, Monkey 2 results show consistent pattern for the lower (<10 Hz) and higher (10-50 Hz) frequency bands.

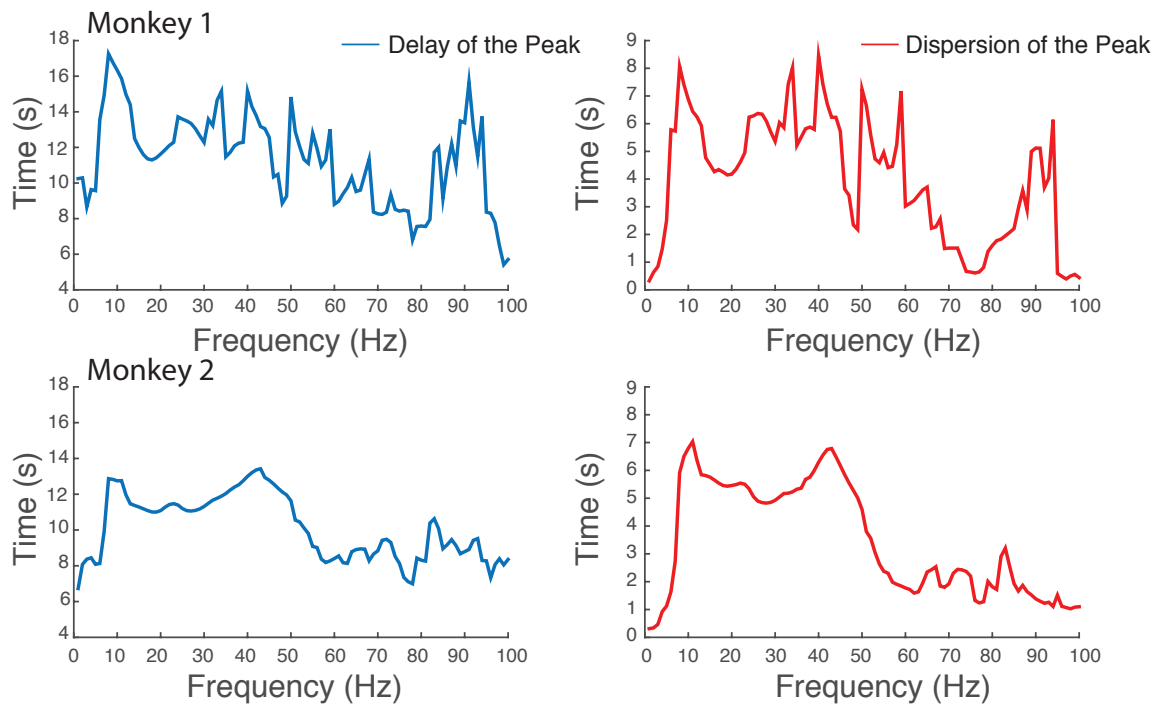


Figure 18: Optimized Values for Delay and Dispersion of the Peak.

3.4 Electrophysiological BLP Regression Analysis

Based on all the analyses so far, the spectrum was divided into two broad BLP bins for further analysis, a “high” (16-44 Hz, beta-low gamma) and a “low” (2-7 Hz, delta-theta) bin. This spectrum division was based on the maximum correlation (positive and negative) observed in figure 10. While there was a positive correlation in the frequency range of 10-50 Hz, the correlation was higher between 16-44 Hz in both animals. On the other hand, the negative correlation was observed in the frequency range of < 10 Hz and the magnitude of the correlation was higher between 2-7 Hz in both animals. Figure 19 displays representative traces of the convolved high and low frequency bins with the averaged positive BOLD network signal time series, illustrating the strong temporal coupling between higher LFP power and BOLD and the negative relationship with low LFP power envelopes.

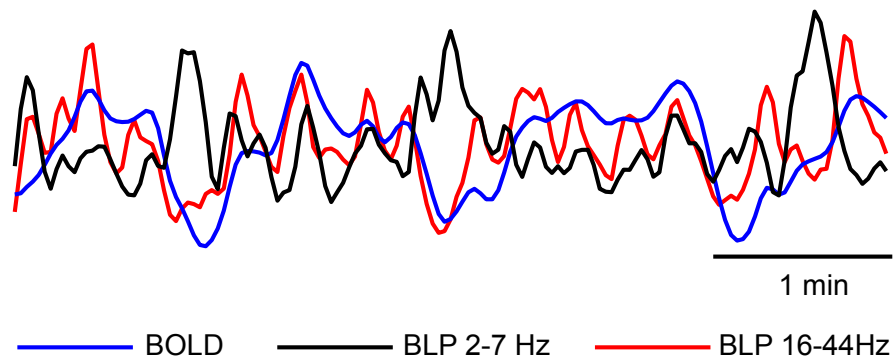


Figure 19: Representative Traces of BOLD, High BLP-LFP and Low BLP-LFP.

The high and low BLP envelopes were used in a regression analysis with BOLD functional images and the resulting connectivity maps matched the maps derived using

the BOLD time series of the electrode seed (Figure 20). While high BLP envelopes revealed the same pattern, low BLP envelopes revealed the opposite pattern: they were strongly anti-correlated with the positive BOLD network pattern observed in seed-based analysis, and were positively coupled to anti-correlated regions in Figure 9 (Figure 21). Figure 22 shows the unflattened surface maps with the same threshold.

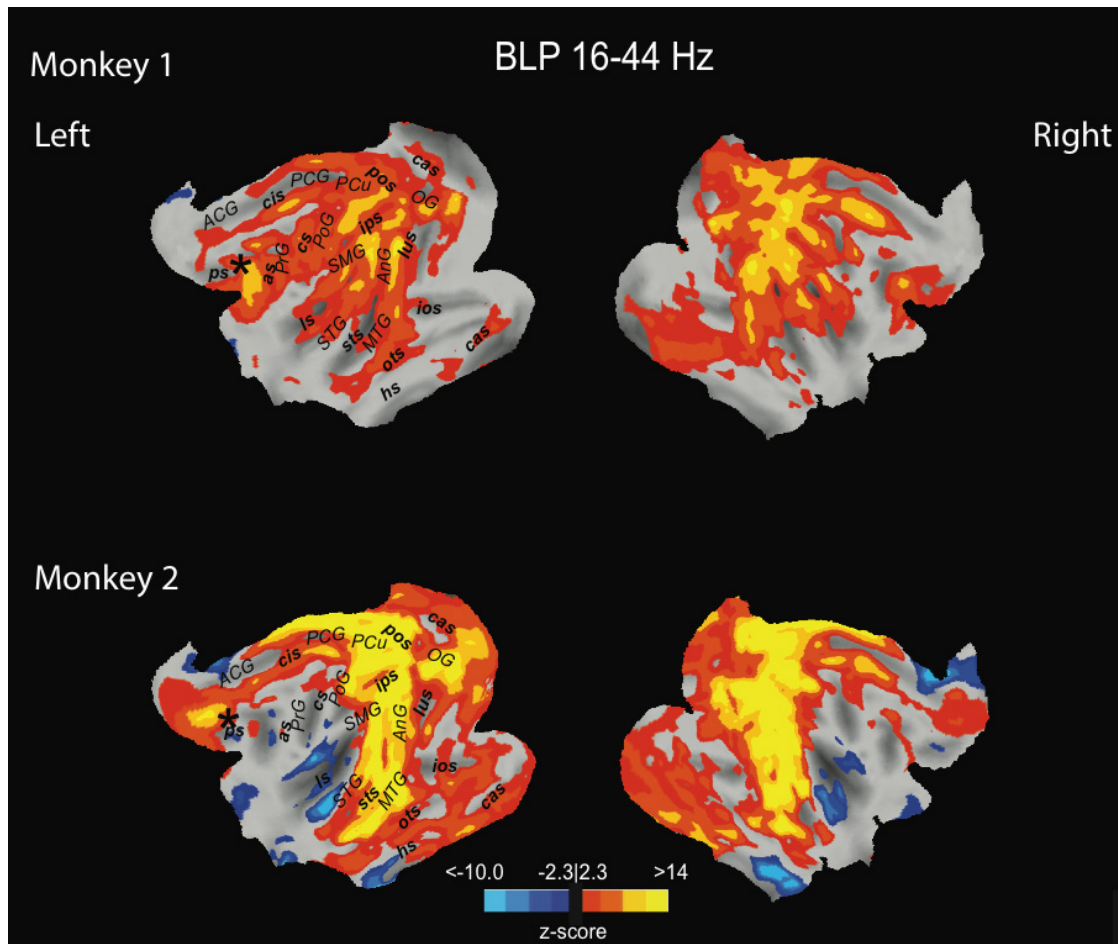


Figure 20: Electrophysiological High BLP Regression Analysis. Voxel-wise, whole-brain regression analysis results are displayed on the flattened left and right hemispheres for each monkey for upper (16-44 Hz) frequency bins ($z > 2.3$; cluster significance: $p < 0.05$, corrected).

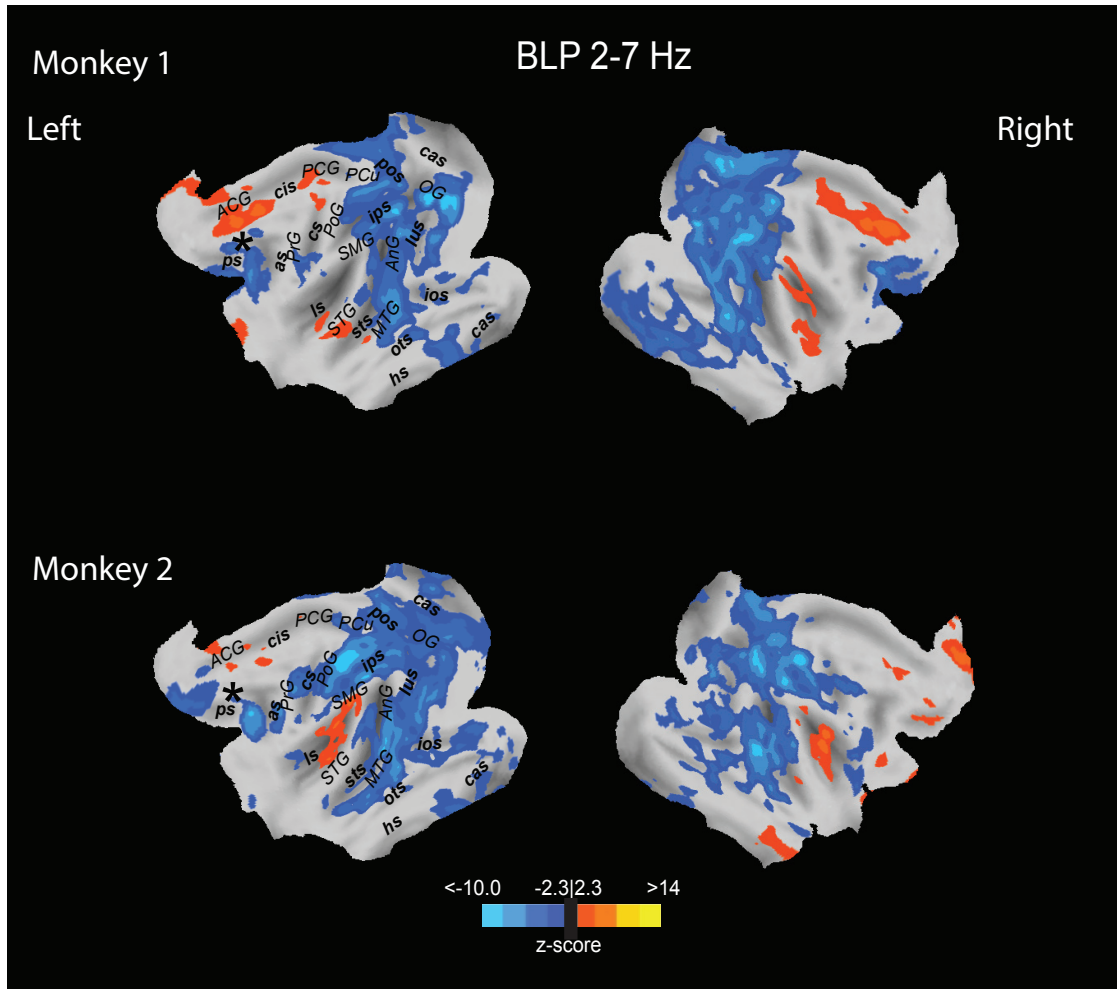


Figure 21: Electrophysiological Low BLP Regression Analysis. Voxel-wise, whole-brain regression analysis results are displayed on the flattened left and right hemispheres for each monkey for lower (2-7 Hz) frequency bins ($z > 2.3$; cluster significance: $p < 0.05$, corrected).

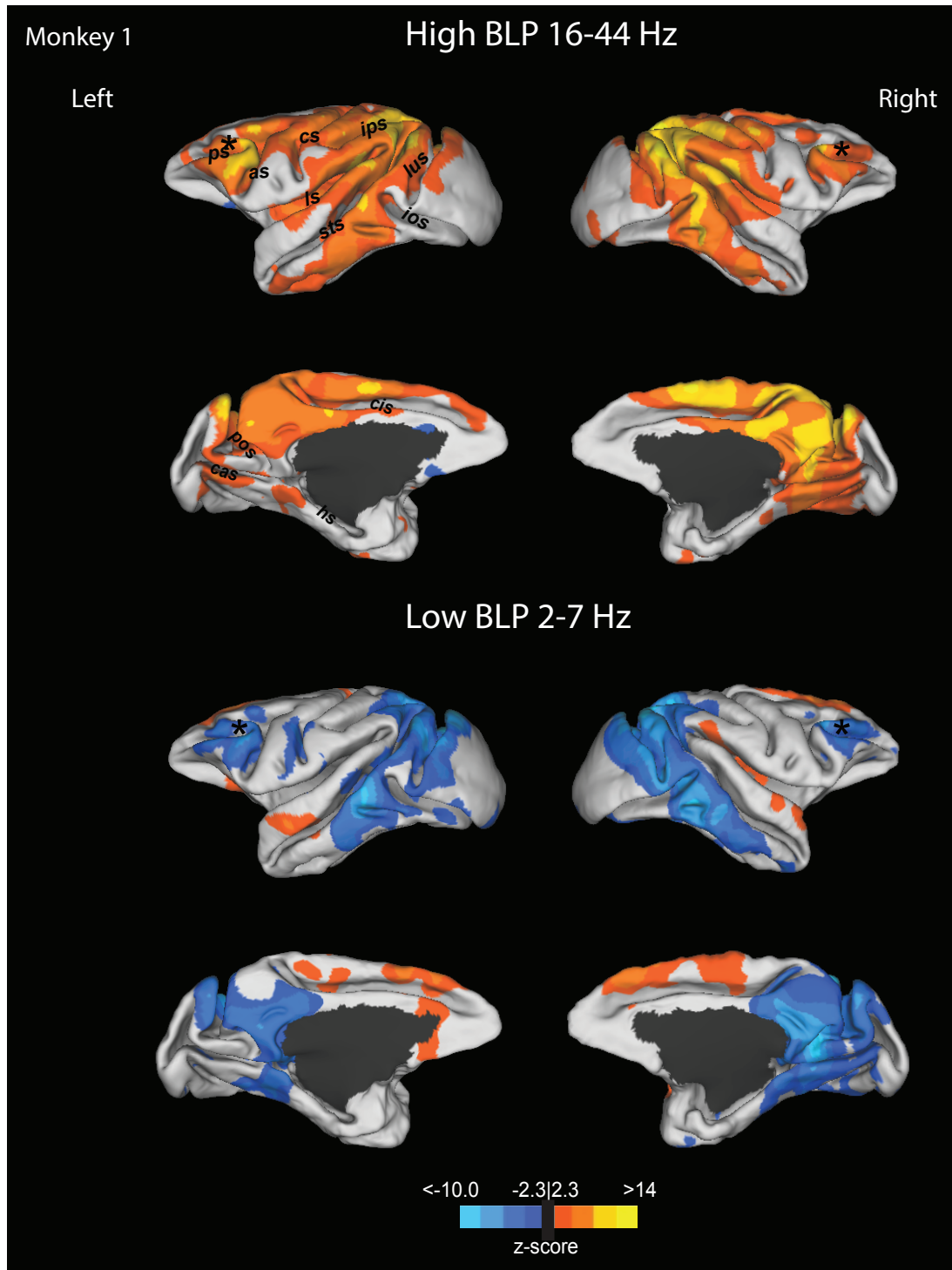


Figure 22: Electrophysiological BLP Regression Analysis on Surface Maps for Monkey 1. Unflattened Functional maps of BOLD and high and low BLP-LFP signals shown in Figure 20 and Figure 21. The maps are displayed on the medial (top) and lateral (bottom) brain surface ($z > 2.3$; cluster significance: $p < 0.05$, corrected).

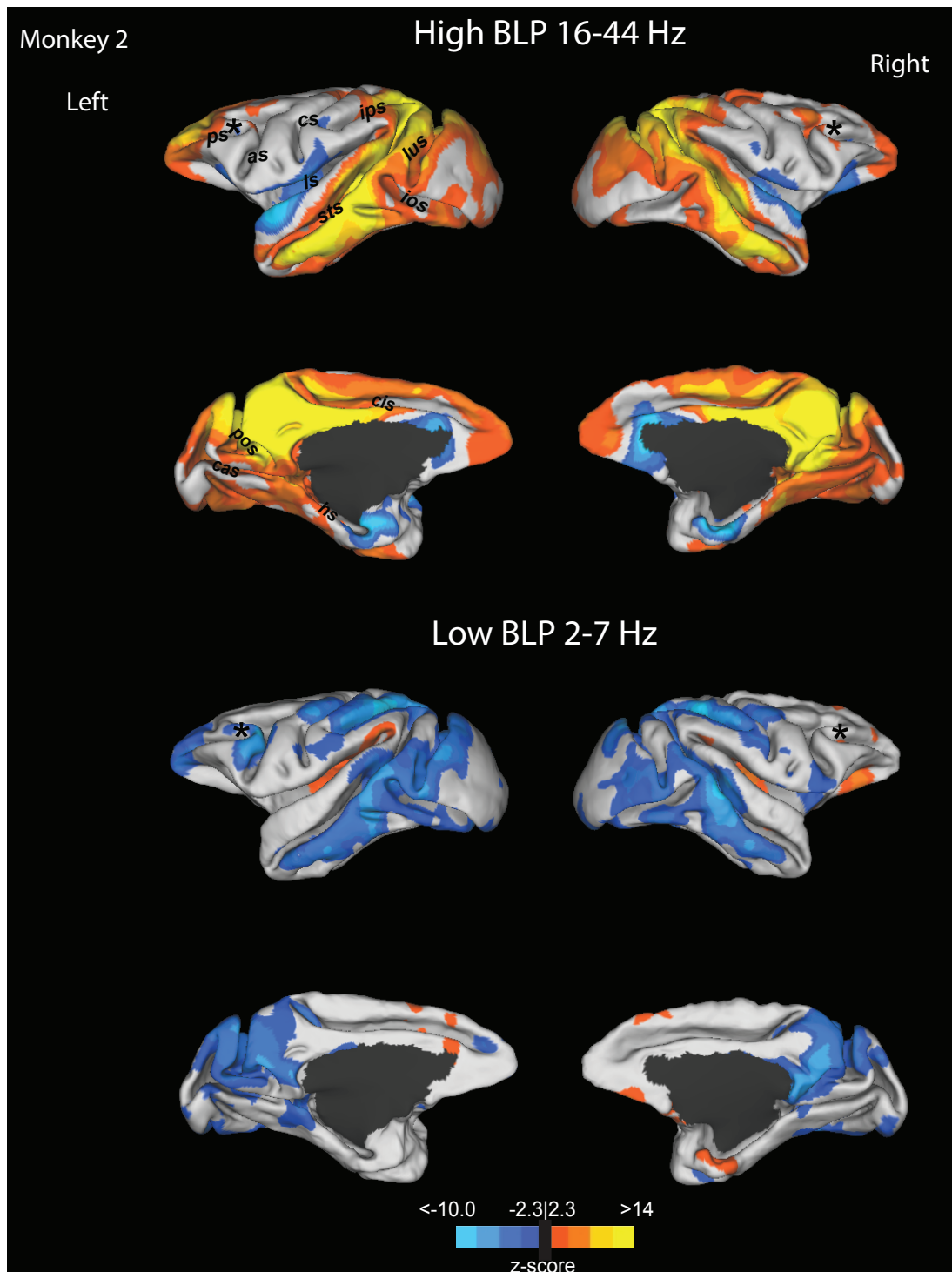


Figure 23: Electrophysiological BLP Regression Analysis on Surface Maps for Monkey 2. Unflattened Functional maps of BOLD and high and low BLP-LFP signals shown in Figure 20 and Figure 21. The maps are displayed on the medial (top) and lateral (bottom) brain surface ($z > 2.3$; cluster significance: $p < 0.05$, corrected).

4 Discussion and Conclusions

As we aimed to investigate the correlation between LFPs and rs-BOLD fMRI signals, the present results demonstrate a widespread correlation between the power of LFPs and BOLD signals in wide frequency bands. Positively and negatively correlated areas observed in BOLD FC profiles exhibit opposite correlations for lower and higher frequency bands. While the signal powers of LFPs were convolved with human HRF, the shape of HRF was optimized in order to best estimate the BOLD fluctuations from the LFPs.

4.1 LFP-BOLD Correlation

Results indicate an anti-correlation between high and low frequency power envelopes of LFPs as the neural origin of positive and negative or anti-correlated networks observed in BOLD FC profiles at rest. While positively connected regions are coupled at higher frequency bands (alpha, beta and low gamma), negatively connected regions are synchronized at lower frequency bands (delta-theta). On the other hand, those positively connected regions are anti-correlated with lower frequency bands and negatively connected regions are anti-correlated with higher frequency bands.

Although anti-correlated interactions observed in BOLD FC profiles have been neglected, our results suggest that both positive and negative FC are correlated with specific neural oscillations, albeit the correlation is stronger for positively connected networks. Since there are reports which discuss global signal regression, a common preprocessing step, introducing negative FC (Murphy et al., 2009), we did not perform GSR in our preprocessing procedure to avoid false positive errors.

To further investigate the LFP-BOLD correlation, we considered another approach to construct the correlation maps based on the GLM. HRF-convolved BLP time series were included as parametric regressors in the GLM. The result of regression analysis on higher frequency power of LFPs and BOLD time series showed similar positive and negative patterns of connectivity to that of seed-based analysis connectivity patterns. Lower frequency power of LFPs revealed a similar spatial pattern with an opposite spectral pattern, being robustly anti-correlated with positive networks observed in the seed-based analysis pattern, which was positively correlated to the negative networks.

To our knowledge, this is the first time that the neural correlate of rs-fMRI is being investigated by simultaneously recorded neural signals such as LFPs from an association (prefrontal) cortex in anesthetized monkeys. There are overlaps between previous studies and our results showing that gamma band exhibits a positive correlation with BOLD fluctuations (Keller et al., 2013; Niessing et al., 2005; Scheeringa et al., 2011; Schölvinck et al., 2010; Shmuel and Leopold, 2008). While these studies showed the highest correlation for high gamma band, our results show that lower gamma band is more correlated to the BOLD signal.

Gamma band activity (GBA) (30-90 Hz) and the neural synchronization in this frequency range have been shown to be associated with several cognitive functions (memory, perception, selective memory, motivation and behavioral control) across many cortical and subcortical areas (Bosman et al., 2014). Cortical gamma oscillations result from the interplay between synaptic excitation produced by glutamatergic neurons and inhibition produced by GABAergic neurons (Buzsáki and Wang, 2012). More generally,

interneuron-interneuron or pyramidal cell-interneuron interactions give rise to gamma oscillations in many cortical areas as they contribute to different functions.

While a general relationship between GBA in PFC and working memory has been shown (Salazar et al., 2012), LFP recordings in lateral PFC in monkeys show a more specific function for GBA as phase-coding of information (Siegel et al. 2009). In visual cortex, GBA contributes to feature integration and visual selective attention tasks (Fries et al., 2001).

From an evolutionary perspective, GBA has been observed in evolutionary divergent species (Buzsáki et al., 2013). It is proposed that increase in brain size and reshaping of neural architecture were accompanied throughout the evolution in order to keep the communication timing the same in different brain areas and this hypothesis relate to the preserved GBA across different species. In overall, gamma oscillation can be associated with low-level functions such as phase-coding in circuit computation, and at a higher level with cognitive functions such as visual processing (Bosman et al., 2014).

There is less consistency with regards to our results from the lower frequency bands and their contribution to fMRI slow fluctuations (to review Engel et al., 2013; Leopold and Maier, 2012; Siegel et al., 2012). Moreover, spatial pattern of LFP-BOLD correlation corresponds to BOLD FC pattern and it is not global as has been suggested before (Schölvinck et al., 2010). In fact, the correlation has a spatial pattern that mostly reflects anatomical connectivity between the regions involved in the FC profiles.

All of these findings support the idea that the hemodynamics of different brain regions are highly correlated to ongoing neural activities at rest and these network-specific brain

rhythms are the fingerprints of the fact that the brain is always active (Mantini et al., 2007).

4.2 Effect of HRF Variation on LFP-BOLD Correlation

As described in chapter one introduction, future studies must convey the HRF variation issues. It is important that this active area of research moves forward so we can better analyze and interpret fMRI data. One main issue is how much the HRF variation affects the results drawn from fMRI studies.

In our study, we convolved the band-passed filtered power of LFPs with the SPM double gamma HRF to estimate the BOLD time series. This function has seven parameters namely: delay and dispersion of the peak, delay and dispersion of the post-stimulus undershoot, peak to undershoot ratio, onset of the response and length of kernel. The parameters were subsequently varied from their default values within biological limits for different brain regions.

While, delay of the peak, peak to undershoot ratio and the response onset had considerable effects on LFP-BOLD correlation, dispersion of the peak had a very mild effect and the rests had no effect at all. Besides this approach, an optimization technique was applied to see the effect of variations of related parameters such as delay and dispersion of the peak. Interestingly, a very similar pattern to the previous results (maximum of 0.45 correlation) with higher correlation (maximum of 0.6 correlation) was obtained here.

As a result, we found that SPM's double gamma HRF is reasonable for convolving the spontaneous neural fluctuations that were simultaneously recorded with fMRI and there

was no considerable difference between the optimal HRF for different brain regions. In fact, consistent with some previous studies (Handwerker et al., 2004; Zumer et al., 2010), we did not find it critical to use region-specific HRF because of following reasons: first, a high-field MRI, like a 7-T scanner is thought to be more sensitive to local microvasculature changes rather than the magnetic distortions induced by large veins (Ugurbil et al., 1999). Therefore, the magnetic susceptibility, which is generally one of the causes of HRF variation, was not a concern here. Second, the results of correlation analysis showed a high similarity for different HRFs. Overall, a misspecification of HRF is a minimum concern here.

4.3 Resting-State fMRI Confounds

Because of the nature of rs-fMRI signals that come from spontaneous activities of the brain, indirectly measuring the neuronal activation, many non-neuronal sources can influence the measure of functional connectivity. Some of these confounds originate from physiological phenomena like motion, cardiac and respiratory cycles, blood pressure, cerebral auto-regulation and vasomotion and some are related to MR physics (Murphy et al., 2013).

One kind of motion artifact that is problematic in fMRI is head motion that changes the uniformity of the magnetic field. Since the animals were anesthetized and their heads were fully stabilized inside the scanner, we did not observe head motion artifacts to be a problem in this study. This was assured by omitting MC confounds in GLM, so we did not see any significant difference compared to the results where MC confounds were added to the model. However, we were forced to deal with movements of the LFP

recording cables and connectors that induced variable artifacts that could not be removed by AAS technique resulting in loss of some data.

Head motion is not the only source of movement artifact. The subject's chest movement while breathing in and out alters the magnetic field (Brosch et al., 2002). Movements in and around large blood vessels due to cardiac pulsation also distort the magnetic field. These two cycles push the brain stem into adjacent brain tissue and result in CSF and WM movement (Dagli et al., 1999). This is the rationale of partialling out the WM and CSF confounds when correlating the BOLD signal to LFPs. On the other hand, respiration and cardiac cycles are about 0.3 and 1 Hz respectively. They are filtered out in preprocessing procedures, as the fMRI data was low-pass filtered by 2.8 s (0.36 Hz) and high-pass filtered by 100s (0.01 Hz).

Cerebral auto-regulation is an intrinsic ability of blood vessels to maintain the stability of CBF in spite of blood pressure fluctuations that are controlled by the nervous system. This is performed by vasoconstriction and vasodilation processes in the vasculature system of the human body (Failla et al., 1999). Besides this, vasomotion fluctuations that rise from contractions of smooth muscle of the arterioles also show low frequency oscillations (< 0.1 Hz) (Aalkjær et al., 2011).

With current technology, it is not possible to remove all confounds. But with external recording of physiological confounds and data-based cleanups such as filtering and GSR, we can only reduce the variance in fMRI data to some extent and increase the statistical power of analysis to better interpret outcomes. Physiological recordings can be utilized in a linear regression analysis to estimate the data. Meanwhile, when choosing a cleanup

method one should take into consideration that some of these confounds have neural bases and removing them will result in removing the signal of interest as well (Murphy et al., 2013).

4.4 Effect of Anesthetics on Brain Functional Architecture

Isoflurane and other anesthetics induce alterations in neural, neurovascular and BOLD signals (Hutchison et al., 2014; Masamoto et al., 2007; Vincent et al., 2007). However, the results from dose-dependent analyses show stable FC between 1 to 1.5 % dosages of isoflurane when there is a profound loss of consciousness. The robust spontaneous BOLD fluctuations resemble those patterns from awake conditions (Hutchison et al., 2014; Vincent et al., 2007) and it has been shown that BOLD FC networks are robust to global state changes (Engel et al., 2013).

While we performed fMRI on non-human primates anesthetized with 1% isoflurane, electrophysiological recording from anesthetized cat primary visual cortex presented a positive correlation between high frequency LFPs (>30 Hz) and BOLD signal and a negative correlation for lower frequency bands (<7 Hz) (Niessing et al., 2005).

4.5 Conclusions

The results reported here describe the neural basis of spontaneous low frequency BOLD fluctuations by means of simultaneously recorded LFPs. We have established that power of LFPs in higher frequency ranges (alpha, beta and low gamma), as a key feature of the neural activity, are highly correlated to positive rs-BOLD networks. Meanwhile, LFP power in lower frequency bands (delta and theta) show anti-correlation to these networks and positive correlation to the anti-correlated rs-BOLD networks. While observed anti-

correlated or antagonistic networks in BOLD profiles are thought to be introduced by preprocessing steps of fMRI analysis such as GSR, there are robust antagonistic networks such as DMN and dorsal-attention networks that disprove this hypothesis. Above findings suggest that unique LFP oscillations are linked to both types of these networks and contribute to them differently.

There is evidence demonstrating that region- or subject-specific HRFs can alter the results drawn from fMRI analysis. Meanwhile, simulations have shown only slight improvements with specific HRFs compared with canonical HRF, which is used in SPM by default. Our results show a very robust and consistent HRF model used for the average of positive and negative BOLD networks derived by seed-based analysis in area 9/46d (Figure 13-14), the FEF in Monkey 1 (Figure 15) and area 7m in Monkey 2 (Figure 16). Optimizing the HRF parameters support the idea that LFP-BOLD correlation is robust to HRF variations as well.

The brain function and the correlation between spontaneous BOLD fluctuations and neuronal activations happening in several brain networks can be assessed by multimodal techniques such as simultaneous LFP-fMRI recording. However, the neural correlates underlying BOLD fluctuations are not yet fully understood. Monkey fMRI is playing a crucial role here and there is evidence demonstrating the similarity of brain function and anatomical connection between these two species. On the other hand, some studies argue about the discrepancy between the electrophysiology of human and monkey brains as the cause of differences in fMRI or electrophysiology results (Kagan et al., 2010). However, due to subject and ethical limitations, monkey fMRI seems to be of great importance to facilitate these investigations.

Studying resting state brain functionality can open new paths to understand the underlying mechanisms of several neurological and psychological disorders. In the future, to gain a deeper insight into the neural correlates of spontaneous BOLD FC at rest, having a larger number of subjects implanted with electrodes in multiple regions of the brain is necessary. Recording LFPs from different regions will also allow us to better generalize the correlation patterns observed between BOLD and LFP fluctuations.

References

- Aalkjær, C., Boedtkjer, D., Matchkov, V., 2011. Vasomotion - what is currently thought? *Acta Physiol* 202, 253–269.
- Allen, P.J., Polizzi, G., Krakow, K., Fish, D.R., Lemieux, L., 1998. Identification of EEG events in the MR scanner: the problem of pulse artifact and a method for its subtraction. *Neuroimage* 8, 229–239.
- Anand, A., Li, Y., Wang, Y., Wu, J., Gao, S., Bukhari, L., Mathews, V.P., Kalnin, A., Lowe, M.J., 2005. Activity and connectivity of brain mood regulating circuit in depression: a functional magnetic resonance study. *Biol. Psychiatry* 57, 1079–1088.
- Attwell, D., Laughlin, S.B., 2001. An energy budget for signaling in the grey matter of the brain. *J. Cerebral Blood Flow & metabolism* 21, 1133-1145.
- Azouz, R., Gray, C.M., 1999. Cellular mechanisms contributing to response variability of cortical neurons in vivo. *J. Neurosci* 19, 2209–2223.
- Barenne, J. D., & McCulloch, W. S., 1938. The direct functional interrelation of sensory cortex and optic thalamus. *J. Neurophysiol* 1, 176-186.
- Beckmann, C.F., DeLuca, M., Devlin, J.T., Smith, S.M., 2005. Investigations into resting-state connectivity using independent component analysis. *Philos. Trans. R. Soc. Lond. B. Biol. Sci.* 360, 1001–1013.
- Bettus, G., Ranjeva, J.-P., Wendling, F., Bénar, C.G., Confort-Gouny, S., Régis, J., Chauvel, P., Cozzone, P.J., Lemieux, L., Bartolomei, F., Guye, M., 2011. Interictal functional connectivity of human epileptic networks assessed by intracerebral EEG and BOLD signal fluctuations. *PLoS One* 6, e20071.
- Biswal, B.B., Mennes, M., Zuo, X.-N., Gohel, S., Kelly, C., Smith, S.M., Beckmann, C.F., Adelstein, J.S., Buckner, R.L., Colcombe, S., Dogonowski, A.-M., Ernst, M., Fair, D., Hampson, M., Hoptman, M.J., Hyde, J.S., Kiviniemi, V.J., Kötter, R., Li, S.-J., Lin, C.-P., Lowe, M.J., Mackay, C., Madden, D.J., Madsen, K.H., Margulies,

- D.S., Mayberg, H.S., McMahon, K., Monk, C.S., Mostofsky, S.H., Nagel, B.J., Pekar, J.J., Peltier, S.J., Petersen, S.E., Riedl, V., Rombouts, S. a R.B., Rypma, B., Schlaggar, B.L., Schmidt, S., Seidler, R.D., Siegle, G.J., Sorg, C., Teng, G.-J., Veijola, J., Villringer, A., Walter, M., Wang, L., Weng, X.-C., Whitfield-Gabrieli, S., Williamson, P., Windischberger, C., Zang, Y.-F., Zhang, H.-Y., Castellanos, F.X., Milham, M.P., 2010. Toward discovery science of human brain function. *Proc. Natl. Acad. Sci. U. S. A.* 107, 4734–4739.
- Biswal, B., Yetkin, F.Z., Haughton, V.M., Hyde, J.S., 1995. Functional connectivity in the motor cortex of resting. *MRM* 34, 537–541.
- Bluhm, R.L., Miller, J., Lanius, R. a, Osuch, E. a, Boksman, K., Neufeld, R.W.J., Théberge, J., Schaefer, B., Williamson, P., 2007. Spontaneous low-frequency fluctuations in the BOLD signal in schizophrenic patients: anomalies in the default network. *Schizophr. Bull.* 33, 1004–1012.
- Bosman, C. A., Lansink, C. S., Pennartz, C., 2014. Functions of gamma-band synchronization in cognition: from single circuits to functional diversity across cortical and subcortical systems. *European Journal of Neuroscience* 39, 1982-1999.
- Britz, J., Van De Ville, D., Michel, C.M., 2010. BOLD correlates of EEG topography reveal rapid resting-state network dynamics. *Neuroimage* 52, 1162–1170.
- Brodmann, K., 1909. *Brodmann's Localisation in the Cerebral Cortex*. Springer Science.
- Brosch, J.R., Talavage, T.M., Ulmer, J.L., Nyenhuis, J.A., Member, S., 2002. Simulation of human respiration in fMRI with a mechanical model. *IEEE Trans. Biomed. Eng.* 49, 700–707.
- Buchwald, J. S., Grover, F. S., 1970. Amplitudes of background fast activity characteristic of specific brain sites. *J Neurophysiol* 33, 148-159.

- Buchwald, J. S., Hala, E. S., Schramm, S., 1965. A comparison of multi-unit activity and EEG activity recorded from the same brain site in chronic cats during behavioral conditioning. *Nature*, 205, 1012-1014.
- Bullmore, E., Sporns, O., 2009. Complex brain networks: graph theoretical analysis of structural and functional systems. *Nat. Rev. Neurosci.* 10, 186–198.
- Bush, K., Cisler, J., 2013. Decoding neural events from fMRI BOLD signal: a comparison of existing approaches and development of a new algorithm. *Magn. Reson. Imaging* 31, 976–89.
- Buxton, R.B., 2001. The elusive initial dip. *Neuroimage* 13, 953–958.
- Buxton, R.B., Uludağ, K., Dubowitz, D.J., Liu, T.T., 2004. Modeling the hemodynamic response to brain activation. *Neuroimage* 23, 220–233.
- Buzsáki, G., Logothetis, N.K. Singer, W., 2013. Scaling brain size, keeping timing: evolutionary preservation of brain rhythms. *Neuron* 80, 751–764.
- Buzsáki, G., Wang, X. J., 2012. Mechanisms of gamma oscillations. *Annual Review of Neuroscience* 35, 203.
- Castellanos, F.X., Margulies, D.S., Kelly, A.M.C., Uddin, L.Q., Ghaffari, M., Kirsch, A., Shaw, D., Shehzad, Z., Martino, A. Di, Biswal, B., Edmund, J., Rotrosen, J., Adler, L.A., Milham, M.P., 2009. Cingulate-precuneus interactions: a new locus of dysfunction in adult attention-deficit/hyperactivity disorder. *NIH Public Access* 63, 332–337.
- Centeno, M., Carmichael, D.W., 2014. Network connectivity in epilepsy: resting state fMRI and EEG-fMRI contributions. *Front. Neurol.* 5, 93.
- Cordes, D., Haughton, V.M., Arfanakis, K., Wendt, G.J., Turski, P.A., Moritz, C.H., Quigley, M.A., Meyerand, M.E., 2000. Mapping functionally related regions of brain with functional connectivity MR imaging. *AJNR Am. J. Neuroradiol.* 21, 1636–1644.

- Crosson, P.L., Johansen-Berg, H., Behrens, T.E.J., Robson, M.D., Pinski, M. a, Gross, C.G., Richter, W., Richter, M.C., Kastner, S., Rushworth, M.F.S., 2005. Quantitative investigation of connections of the prefrontal cortex in the human and macaque using probabilistic diffusion tractography. *J. Neurosci.* 25, 8854–8866.
- Dagli, M.S., Ingeholm, J.E., Haxby, J. V, 1999. Localization of cardiac-induced signal change in fMRI. *Neuroimage* 9, 407–415.
- Damoiseaux, J.S., Rombouts, S. a R.B., Barkhof, F., Scheltens, P., Stam, C.J., Smith, S.M., Beckmann, C.F., 2006. Consistent resting-state networks across healthy subjects. *Proc. Natl. Acad. Sci. U. S. A.* 103, 13848–13853.
- David, O., Guillemain, I., Sallet, S., Reyt, S., Deransart, C., Segebarth, C., Depaulis, A., 2008. Identifying neural drivers with functional MRI: an electrophysiological validation. *PLoS Biol.* 6, 2683–2697.
- De Luca, M., Beckmann, C.F., De Stefano, N., Matthews, P.M., Smith, S.M., 2006. fMRI resting state networks define distinct modes of long-distance interactions in the human brain. *Neuroimage* 29, 1359–67.
- Doesburg, S.M., Green, J.J., McDonald, J.J., Ward, L.M., 2009. From local inhibition to long-range integration: a functional dissociation of alpha-band synchronization across cortical scales in visuospatial attention. *Brain Res.* 1303, 97–110.
- Douglas, R. J., Martin, K. A., 2004. Neuronal circuits of the neocortex. *Annu. Rev. Neurosci.* 27, 419-451.
- Duvernoy, H. M., Delon, S., Vannson, J. L., 1981. Cortical blood vessels of the human brain. *Brain research bulletin* 7, 519-579.
- Engel, A.K., Gerloff, C., Hilgetag, C.C., Nolte, G., 2013. Intrinsic coupling modes: multiscale interactions in ongoing brain activity. *Neuron* 80, 867–886.

- Failla, M., Grappiolo, A., Emanuelli, G., Vitale, G., Fraschini, N., Bigoni, M., Grieco, N., Denti, M., Giannattasio, C., Mancina, G., 1999. Sympathetic tone restrains arterial distensibility of healthy and atherosclerotic subjects. *J. Hypertens.* 17, 1117–1123.
- Farber, N. E., Harkin, C. P., Niedfeldt, J., Hudetz, A. G., Kampine, J. P., Schmeling, W. T., 1997. Region-specific and agent-specific dilation of intracerebral microvessels by volatile anesthetics in rat brain slices. *Anesthesiology* 87, 1191-1198.
- Fox, M.D., Raichle, M.E., 2007. Spontaneous fluctuations in brain activity observed with functional magnetic resonance imaging. *Nat. Rev. Neurosci.* 8, 700–711.
- Fox, P. T., Raichle, M. E., Mintun, M. A., Dence, C. , 1988. Nonoxidative glucose consumption during focal physiologic neural activity. *Science* 241, 462-464.
- Fries, P., Reynolds, J.H., Rorie, A.E., Desimone, R., 2001. Modulation of oscillatory neuronal synchronization by selective visual attention 291, 1560-1563.
- Friston, K., 2003. Statistical Parametric Mapping. *Neuroscience Databases*. Springer US, 237-250.
- Gilbert, C. D., 1983. Microcircuitry of the visual cortex. *Annual review of neuroscience* 6, 217-247.
- Godlove, D. C., Maier, A., Woodman, G. F., Schall, J. D., 2014. Microcircuitry of agranular frontal cortex: testing the generality of the canonical cortical microcircuit. *The Journal of Neuroscience* 34, 5355-5369.
- Goense, J.B.M., Logothetis, N.K., 2008. Neurophysiology of the BOLD fMRI signal in awake monkeys. *Curr. Biol.* 18, 631–640.
- Gonzalez-Castillo, J., Saad, Z.S., Handwerker, D. a, Inati, S.J., Brenowitz, N., Bandettini, P. a, 2012. Whole-brain, time-locked activation with simple tasks revealed using massive averaging and model-free analysis. *Proc. Natl. Acad. Sci. U. S. A.* 109, 5487–5492.

- Gray, C. M., König, P., Engel, A. K., Singer, W., 1989. Oscillatory responses in cat visual cortex exhibit inter-columnar synchronization which reflects global stimulus properties. *Nature* 338, 334-337.
- Greicius, M., 2008. Resting-state functional connectivity in neuropsychiatric disorders. *Curr. Opin. Neurol.* 21, 424–430.
- Greicius, M.D., Srivastava, G., Reiss, A.L., Menon, V., 2004. Default-mode network activity distinguishes Alzheimer’s disease from healthy aging: evidence from functional MRI. *Proc. Natl. Acad. Sci. U. S. A.* 101, 4637–4642.
- Gross, J., Schmitz, F., Schnitzler, I., Kessler, K., Shapiro, K., Hommel, B., Schnitzler, A., 2004. Modulation of long-range neural synchrony reflects temporal limitations of visual attention in humans. *Proc. Natl. Acad. Sci. U. S. A.* 101, 13050–13055.
- Hagmann, P., Cammoun, L., Gigandet, X., Meuli, R., Honey, C.J., Wedeen, V.J., Sporns, O., 2008. Mapping the structural core of human cerebral cortex. *PLoS Biol.* 6, e159.
- Handwerker, D. a, Ollinger, J.M., D’Esposito, M., 2004. Variation of BOLD hemodynamic responses across subjects and brain regions and their effects on statistical analyses. *Neuroimage* 21, 1639–1651.
doi:10.1016/j.neuroimage.2003.11.029
- Havlicek, M., Friston, K.J., Jan, J., Brazdil, M., Calhoun, V.D., 2011. Dynamic modeling of neuronal responses in fMRI using cubature Kalman filtering. *Neuroimage* 56, 2109–2128.
- He, B.J., Snyder, A.Z., Zempel, J.M., Smyth, M.D., Raichle, M.E., 2008. Electrophysiological correlates of the brain’s intrinsic large-scale functional architecture. *Proc. Natl. Acad. Sci. U. S. A.* 105, 16039–1644.
- Heeger, D.J., Ress, D., 2002. What does fMRI tell us about neuronal activity? *Nat. Rev. Neurosci.* 3, 142–151.

- Hodgkin, a. L., Huxley, a. F., 1952. Propagation of electrical signals along giant nerve fibres. *Proc. R. Soc. B Biol. Sci.* 140, 177–183.
- Honey, C.J., Kotter, R., Breakspear, M., Sporns, O., 2007. Network structure of cerebral cortex shapes functional connectivity on multiple time scales. *Proc. Natl. Acad. Sci. U. S. A.* 104, 10240–10245.
- Honey, C.J., Sporns, O., Cammoun, L., Gigandet, X., Thiran, J.P., Meuli, R., Hagmann, P., 2009. Predicting human resting-state functional connectivity from structural connectivity. *Proc. Natl. Acad. Sci. U. S. A.* 106, 2035–2040.
- Hong, L.E., Buchanan, R.W., Thaker, G.K., Shepard, P.D., Summerfelt, A., 2008. Beta (~16 Hz) frequency neural oscillations mediate auditory sensory gating in humans. *Psychophysiology* 45, 197–204.
- Horowitz, S.G., Fukunaga, M., de Zwart, J. a, van Gelderen, P., Fulton, S.C., Balkin, T.J., Duyn, J.H., 2008. Low frequency BOLD fluctuations during resting wakefulness and light sleep: a simultaneous EEG-fMRI study. *Hum. Brain Mapp.* 29, 671–682.
- Huerta, P. T., Lisman, J. E., 1993. Heightened synaptic plasticity of hippocampal CA1 neurons during a cholinergically induced rhythmic state. *Nature* 364, 723–725
- Huettel, S. A., Song, A. W., McCarthy, G., 2004. *Functional magnetic resonance imaging (Vol. 1)*. Sunderland, MA: Sinauer Associates.
- Hutchison, R.M., Everling, S., 2012. Monkey in the middle: why non-human primates are needed to bridge the gap in resting-state investigations. *Front. Neuroanat.* 6, 29.
- Hutchison, R.M., Everling, S., 2014. Broad intrinsic functional connectivity boundaries of the macaque prefrontal cortex. *Neuroimage* 88C, 202–211.
- Hutchison, R.M., Gallivan, J.P., Culham, J.C., Gati, J.S., Menon, R.S., Everling, S., 2012. Functional connectivity of the frontal eye fields in humans and macaque monkeys investigated with resting-state fMRI. *J. Neurophysiol.* 107, 2463–2474.

- Hutchison, R.M., Hutchison, M., Manning, K.Y., Menon, R.S., Everling, S., 2014. Isoflurane induces dose-dependent alterations in the cortical connectivity profiles and dynamic properties of the brain's functional architecture. *Hum. Brain Mapp.* 35, 5754-5775.
- Hutchison, R.M., Leung, L.S., Mirsattari, S.M., Gati, J.S., Menon, R.S., Everling, S., 2011. Resting-state networks in the macaque at 7 T. *Neuroimage* 56, 1546–1555.
- Hutchison, R.M., Mirsattari, S.M., Jones, C.K., Gati, J.S., Leung, L.S., 2010. Functional networks in the anesthetized rat brain revealed by independent component analysis of resting-state fMRI. *J. Neurophysiol.* 103, 3398–3406.
- Hutchison, R.M., Womelsdorf, T., Gati, J.S., Everling, S., Menon, R.S., 2013. Resting-state networks show dynamic functional connectivity in awake humans and anesthetized macaques. *Hum. Brain Mapp.* 34, 2154–2177.
- Iadecola, C., Yang, G., Ebner, T. J., Chen, G., 1997. Local and propagated vascular responses evoked by focal synaptic activity in cerebellar cortex. *Journal of neurophysiology* 78, 651-659.
- James, W., 1890. *The principles of psychology*. Harvard UP, Cambridge, MA.
- Jann, K., Kottlow, M., Dierks, T., Boesch, C., Koenig, T., 2010. Topographic electrophysiological signatures of fMRI Resting State Networks. *PLoS One* 5, e12945.
- Jones, M., Berwick, J., Johnston, D., Mayhew, J., 2001. Concurrent optical imaging spectroscopy and laser-Doppler flowmetry: the relationship between blood flow, oxygenation, and volume in rodent barrel cortex. *Neuroimage* 13, 1002–1015.
- Kagan, I., Iyer, A., Lindner, A., Andersen, R. A., 2010. Space representation for eye movements is more contralateral in monkeys than in humans. *Proc. Natl. Acad. Sci. U. S. A.* 107, 7933-7938.

- Keller, C.J., Bickel, S., Honey, C.J., Groppe, D.M., Entz, L., Craddock, R.C., Lado, F. a, Kelly, C., Milham, M., Mehta, A.D., 2013. Neurophysiological investigation of spontaneous correlated and anticorrelated fluctuations of the BOLD signal. *J. Neurosci.* 33, 6333–6342.
- Kilner, J.M., Baker, S.N., Salenius, S., Hari, R., Lemon, R.N., 2000. Human cortical muscle coherence is directly related to specific motor parameters. *J. Neurosci.* 20, 8838–8845.
- Klimesch, W., Sauseng, P., Hanslmayr, S., 2007. EEG alpha oscillations: the inhibition-timing hypothesis. *Brain Res. Rev.* 53, 63–88.
- Koch, M. a, Norris, D.G., Hund-Georgiadis, M., 2002. An investigation of functional and anatomical connectivity using magnetic resonance imaging. *Neuroimage* 16, 241–250.
- Kopell, N., Ermentrout, G.B., Whittington, M.A., Traub, R.D., 1999. Gamma rhythms and beta rhythms have different synchronization properties. *Proc. Natl. Acad. Sci. U. S. A.* 97, 1867-1872.
- Kumar, S., Hedges, S.B., 1998. A molecular timescale for vertebrate evolution. *Nature* 392, 917-920.
- Kumar, S., Penny, W., 2014. Estimating neural response functions from fMRI. *Front. Neuroinform.* 8, 48.
- Lachaux, J.P., Rodriguez, E., Martinerie, J., Varela, F.J., 1999. Measuring phase synchrony in brain signals. *Hum. Brain Mapp.* 8, 194–208.
- Laufs, H., Kleinschmidt, a, Beyerle, a, Eger, E., Salek-Haddadi, a, Preibisch, C., Krakow, K., 2003. EEG-correlated fMRI of human alpha activity. *Neuroimage* 19, 1463–1476.
- Leopold, D. a, Maier, A., 2012. Ongoing physiological processes in the cerebral cortex. *Neuroimage* 62, 2190–2200.

- Leopold, D.A., Murayama, Y., Logothetis, N.K., Planck, M., 2003. Very slow activity fluctuations in monkey visual cortex : implications for functional brain imaging. *Cereb. Cortex* 13, 422–433.
- Liang, Z., King, J., Zhang, N., 2011. Uncovering intrinsic connective architecture of functional networks in awake rat brain. *J. Neurosci.* 31, 3776–3783.
- Logothetis, N., 2000. Can current fMRI techniques reveal the micro-architecture of cortex?. *Nat. Neurosci.* 3, 413-413.
- Logothetis, N.K., 2002. The neural basis of the blood-oxygen-level-dependent functional magnetic resonance imaging signal. *Philos. Trans. R. Soc. Lond. B. Biol. Sci.* 357, 1003–1037.
- Logothetis, N.K., 2003. The underpinnings of the BOLD functional magnetic resonance imaging signal 23, 3963–3971.
- Logothetis, N.K., Pauls, J., Augath, M., Trinath, T., Oeltermann, A., 2001. Neurophysiological investigation of the basis of the fMRI signal. *Nature* 412, 150-157
- Lowe, M.J., Mock, B.J., Sorenson, J. a, 1998. Functional connectivity in single and multislice echoplanar imaging using resting-state fluctuations. *Neuroimage* 7, 119–132.
- Lowe, M.J., Phillips, M.D., Lurito, J.T., Mattson, D., Dziedzic, M., Mathews, V.P., 2002. Multiple sclerosis : low-frequency temporal blood oxygen level-dependent fluctuations indicate reduced functional connectivity-Initial Results 1. *Radiology* 224, 184-192.
- Magri, C., Schridde, U., Murayama, Y., Panzeri, S., Logothetis, N.K., 2012. The amplitude and timing of the BOLD signal reflects the relationship between local field potential power at different frequencies. *J. Neurosci.* 32, 1395–1407.

- Malonek, D., Grinvald, A., 1996. The imaging spectroscopy reveals the interaction between electrical activity and cortical microcirculation: Implication for optical, pet and MR functional brain imaging. *Science* 272, 551-554.
- Mantini, D., Gerits, A., Nelissen, K., Durand, J.-B., Joly, O., Simone, L., Sawamura, H., Wardak, C., Orban, G. a, Buckner, R.L., Vanduffel, W., 2011. Default mode of brain function in monkeys. *J. Neurosci.* 31, 12954–12962.
- Mantini, D., Perrucci, M.G., Del Gratta, C., Romani, G.L., Corbetta, M., 2007. Electrophysiological signatures of resting state networks in the human brain. *Proc. Natl. Acad. Sci. U. S. A.* 104, 13170–13175.
- Marques, J.P., Kober, T., Krueger, G., van der Zwaag, W., Van de Moortele, P.-F., Gruetter, R., 2010. MP2RAGE, a self bias-field corrected sequence for improved segmentation and T1-mapping at high field. *Neuroimage* 49, 1271–1281.
- Masamoto, K., Kim, T., Fukuda, M., Wang, P., Kim, S.-G., 2007. Relationship between neural, vascular, and BOLD signals in isoflurane-anesthetized rat somatosensory cortex. *Cereb. Cortex* 17, 942–950.
- Mason, M.F., Norton, M.I., Horn, J.D. Van, Wegner, D.M., Scott, T., Macrae, C.N., 2007. Wandering minds: the default network and stimulus-independent thought. *Science* 315, 393-395.
- Melloni, L., Molina, C., Pena, M., Torres, D., Singer, W., Rodriguez, E., 2007. Synchronization of neural activity across cortical areas correlates with conscious perception. *J. Neurosci.* 27, 2858–2865.
- Menon, R.S., Ogawa, S., Hu, X., Strupp, J.P., Anderson, P., Ugurbil, K., 1995. BOLD based functional MRI at 4 Tesla includes a capillary bed contribution: echo-planar imaging correlates with previous optical imaging using intrinsic signals. *Magn. Reson. Med.* 33, 453–459.

- Mitzdorf, U., Psychologie, M., Miinchen, D.U., 1987. Properties of the evoked potential generators: current source-density analysis of visually evoked potentials in the cat cortex. *Int.J. Neurosci* 33, 33–59.
- Murphy, K., Birn, R.M., Bandettini, P. a, 2013. Resting-state fMRI confounds and cleanup. *Neuroimage* 80, 349–359.
- Murphy, K., Birn, R.M., Handwerker, D. a, Jones, T.B., Bandettini, P. a, 2009. The impact of global signal regression on resting state correlations: are anti-correlated networks introduced? *Neuroimage* 44, 893–905.
- Nelson, P. G., 1966. Interaction between spinal motoneurons of the cat. *J. Neurophysiol.* 29, 275-287.
- Niessing, J., Ebisch, B., Schmidt, K.E., Niessing, M., Singer, W., Galuske, R. a W., 2005. Hemodynamic signals correlate tightly with synchronized gamma oscillations. *Science* 309, 948–951.
- Ninomiya, T., Dougherty, K., Godlove, D. C., Schall, J. D., Maier, A., 2015. Microcircuitry of agranular frontal cortex: contrasting laminar connectivity between occipital and frontal areas. *Journal of Neurophysiology*, jn-00624, In Press.
- Nir, Y., Fisch, L., Mukamel, R., Gelbard-Sagiv, H., Arieli, A., Fried, I., Malach, R., 2007. Coupling between neuronal firing rate, gamma LFP, and BOLD fMRI is related to interneuronal correlations. *Curr. Biol.* 17, 1275–1285.
- Nir, Y., Mukamel, R., Dinstein, I., Privman, E., Harel, M., Fisch, L., Gelbard-Sagiv, H., Kipervasser, S., Andelman, F., Neufeld, M.Y., Kramer, U., Arieli, A., Fried, I., Malach, R., 2008. Interhemispheric correlations of slow spontaneous neuronal fluctuations revealed in human sensory cortex. *Nat. Neurosci.* 11, 1100–1108.
- Ogawa, S., Lee, T.M., Kay, A.R., 1990. Brain magnetic resonance imaging with contrast dependent on blood oxygenation 87, 9868–9872.

- Ojemann, G. a, Corina, D.P., Corrigan, N., Schoenfield-McNeill, J., Poliakov, A., Zamora, L., Zanos, S., 2010. Neuronal correlates of functional magnetic resonance imaging in human temporal cortex. *Brain* 133, 46–59.
- Ojemann, G. a, Ojemann, J., Ramsey, N.F., 2013. Relation between functional magnetic resonance imaging (fMRI) and single neuron, local field potential (LFP) and electrocorticography (ECoG) activity in human cortex. *Front. Hum. Neurosci.* 7, 34.
- Palva, S., Linkenkaer-Hansen, K., Näätänen, R., Palva, J.M., 2005. Early neural correlates of conscious somatosensory perception. *J. Neurosci.* 25, 5248–5258.
- Pan, W.-J., Thompson, G., Magnuson, M., Majeed, W., Jaeger, D., Keilholz, S., 2011. Broadband local field potentials correlate with spontaneous fluctuations in functional magnetic resonance imaging signals in the rat somatosensory cortex under isoflurane anesthesia. *Brain Connect.* 1, 119–131.
- Pan, W.-J., Thompson, G.J., Magnuson, M.E., Jaeger, D., Keilholz, S., 2013. Infralow LFP correlates to resting-state fMRI BOLD signals. *Neuroimage* 74, 288–297.
- Passingham, R., 2009. How good is the macaque monkey model of the human brain? *Curr. Opin. Neurobiol.* 19, 6–11.
- Passingham, R.E., Stephan, K.E., Kötter, R., 2002. The anatomical basis of functional localization in the cortex. *Nat. Rev. Neurosci.* 3, 606–616.
- Pauling, L., Coryell, C. D., 1936. The magnetic properties and structure of hemoglobin, oxyhemoglobin and carbonmonoxyhemoglobin. *Proc. Natl. Acad. Sci. U. S. A.* 22, 210.
- Pawela, C.P., Biswal, B.B., Cho, Y.R., Kao, D.S., Jones, S.R., Schulte, M.L., Matloub, H.S., Hudetz, A.G., Hyde, S., 2008. Resting-state functional connectivity of the rat brain. *Magn. Reson. Med.* 59, 1021–1029.
- Pedley, T. A., Traub, R. D., 1990. Physiological basis of the EEG. *Current Practice of Clinical Electroencephalography* 2, 107-137.

- Pereira, F.R.S., Alessio, A., Sercheli, M.S., Pedro, T., Bilevicius, E., Rondina, J.M., Ozelo, H.F.B., Castellano, G., Covolan, R.J.M., Damasceno, B.P., Cendes, F., 2010. Asymmetrical hippocampal connectivity in mesial temporal lobe epilepsy: evidence from resting state fMRI. *BMC Neurosci.* 11, 66.
- Petrides, M., Cadoret, G., Mackey, S., 2005. Orofacial somatomotor responses in the macaque monkey homologue of Broca's area. *Nature* 435, 1235–1238.
- Petrides, M., Pandya, D.N., 1999. Dorsolateral prefrontal cortex : comparative cytoarchitectonic analysis in the human and the macaque brain and corticocortical connection patterns. *Euro. J. Neurosci* 11, 1011–1036.
- Picchioni, D., Horowitz, S.G., Fukunaga, M., Carr, W.S., Meltzer, J. a, Balkin, T.J., Duyn, J.H., Braun, A.R., 2011. Infralow EEG oscillations organize large-scale cortical-subcortical interactions during sleep: a combined EEG/fMRI study. *Brain Res.* 1374, 63–72.
- Power, J.D., Fair, D. a, Schlaggar, B.L., Petersen, S.E., 2010. The development of human functional brain networks. *Neuron* 67, 735–748.
- Paxinos G, Huang X. F., Toga A.W., 2000 *The rhesus monkey brain in stereotaxic coordinates.* San Diego: Academic.
- Pribram, K.H., MacLean, P.D., 1953. Neuronographic analysis of medial and basal cerebral cortex. II. Monkey1. *J. Neurophysiol* 16, 324–340.
- Raichle, M.E., 2010. Two views of brain function. *Trends Cogn. Sci.* 14, 180–190.
- Raichle, M.E., MacLeod, a M., Snyder, a Z., Powers, W.J., Gusnard, D. a, Shulman, G.L., 2001. A default mode of brain function. *Proc. Natl. Acad. Sci. U. S. A.* 98, 676–682.
- Raichle, M.E., Mintun, M. a, 2006. Brain work and brain imaging. *Annu. Rev. Neurosci.* 29, 449–476.

- Rees, G., Friston, K., Koch, C., 2000. A direct quantitative relationship between the functional properties of human and macaque V5. *Nat. Neurosci* 3, 716-723.
- Riera, J.J., Watanabe, J., Kazuki, I., Naoki, M., Aubert, E., Ozaki, T., Kawashima, R., 2004. A state-space model of the hemodynamic approach: nonlinear filtering of BOLD signals. *Neuroimage* 21, 547–567.
- Riera, J. J., Ogawa, T., Goto, T., Sumiyoshi, A., Nonaka, H., Evans, A., Kawashima, R., 2012. Pitfalls in the dipolar model for the neocortical EEG sources. *Journal of neurophysiology* 108, 956-975.
- Rockel, A. J., Hiorns, R. W. , Powell, T. P. S., 1980. The basic uniformity in structure of the neocortex. *Brain* 103, 221-244.
- Roebroeck, A., Formisano, E., Goebel, R., 2011. The identification of interacting networks in the brain using fMRI: model selection, causality and deconvolution. *Neuroimage* 58, 296–302.
- Salazar, R.F., Dotson, N.M., Bressler, S.L. Gray, C.M., 2012. Content- specific fronto-parietal synchronization during visual working memory. *Science* 338, 1097–1100.
- Scheeringa, R., Fries, P., Petersson, K.-M., Oostenveld, R., Grothe, I., Norris, D.G., Hagoort, P., Bastiaansen, M.C.M., 2011. Neuronal dynamics underlying high- and low-frequency EEG oscillations contribute independently to the human BOLD signal. *Neuron* 69, 572–583.
- Schölvinck, M.L., Howarth, C., Attwell, D., 2008. The cortical energy needed for conscious perception. *Neuroimage* 40, 1460–1468.
- Schölvinck, M.L., Leopold, D. a, Brookes, M.J., Khader, P.H., 2013. The contribution of electrophysiology to functional connectivity mapping. *Neuroimage* 80, 297–306.
- Schölvinck, M.L., Maier, A., Ye, F.Q., Duyn, J.H., Leopold, D. a, 2010. Neural basis of global resting-state fMRI activity. *Proc. Natl. Acad. Sci. U. S. A.* 107, 10238-10243.

- Shehzad, Z., Kelly, a M.C., Reiss, P.T., Gee, D.G., Gotimer, K., Uddin, L.Q., Lee, S.H., Margulies, D.S., Roy, A.K., Biswal, B.B., Petkova, E., Castellanos, F.X., Milham, M.P., 2009. The resting brain: unconstrained yet reliable. *Cereb. Cortex* 19, 2209–2229.
- Shen, K., Bezgin, G., Hutchison, R.M., Gati, J.S., Menon, R.S., Everling, S., McIntosh, A.R., 2012. Information processing architecture of functionally defined clusters in the macaque cortex. *J. Neurosci.* 32, 17465–17476.
- Shmuel, A., Leopold, D. a, 2008. Neuronal correlates of spontaneous fluctuations in fMRI signals in monkey visual cortex: Implications for functional connectivity at rest. *Hum. Brain Mapp.* 29, 751–761.
- Siegel, M., Donner, T.H., Engel, A.K., 2012. Spectral fingerprints of large-scale neuronal interactions. *Nat. Rev. Neurosci.* 13, 121–134.
- Siegel, M., Warden, M.R. Miller, E.K., 2009. Phase-dependent neuronal coding of objects in short-term memory. *Proc. Natl. Acad. Sci. U.S.A.* 106, 21341–21346.
- Stein, A. Von, Chiang, C., Ko, P., 2000. Top-down processing mediated by interareal synchronization. *Proc. Natl. Acad. Sci. U. S. A.* 97, 14748-14753.
- Tallon-baudry, C., Bertrand, O., Peronnet, F., Pernier, J., Lyon, F., 1998. Induced gamma band activity during the delay of a visual short-term memory task in humans. *The Journal of Neuroscience* 18, 4244–4254.
- Thompson, G.J., Pan, W.-J., Magnuson, M.E., Jaeger, D., Keilholz, S.D., 2014. Quasi-periodic patterns (QPP): large-scale dynamics in resting state fMRI that correlate with local infraslow electrical activity. *Neuroimage* 84, 1018–1031.
- Thut, G., Nietzel, A., Brandt, S. a, Pascual-Leone, A., 2006. Alpha-band electroencephalographic activity over occipital cortex indexes visuospatial attention bias and predicts visual target detection. *J. Neurosci.* 26, 9494–9502.

- Traub, R. D., Whittington, M. A., Stanford, I. M., Jefferys, J. G., 1996. A mechanism for generation of long-range synchronous fast oscillations in the cortex. *Nature* 383, 621-624.
- Ugurbil, K., Xiaoping, H., Wei, C., Zhu, X. H., Kim, S. G., Georgopoulos, A., 1999. Functional mapping in the human brain using high magnetic fields. *Philosophical Transactions of the Royal Society of London. Series B: Biological Sciences* 354, 1195-1213.
- Uhlhaas, P.J., Singer, W., 2010. Abnormal neural oscillations and synchrony in schizophrenia. *Nat. Rev. Neurosci.* 11, 100–113.
- Van Essen, D.C., 2004. Surface-based approaches to spatial localization and registration in primate cerebral cortex. *Neuroimage* 23, 97–107.
- Van Essen, D. C., Drury, H. A., Dickson, J., Harwell, J., Hanlon, D., Anderson, C. H., 2001. An integrated software suite for surface-based analyses of cerebral cortex. *J. Am. Med. Inform. Assoc.* 8, 443–459.
- Vertes, R.P., 2005. Hippocampal theta rhythm: a tag for short-term memory. *Hippocampus* 15, 923–35.
- Vincent, J.L., Patel, G.H., Fox, M.D., Snyder, a Z., Baker, J.T., Van Essen, D.C., Zempel, J.M., Snyder, L.H., Corbetta, M., Raichle, M.E., 2007. Intrinsic functional architecture in the anaesthetized monkey brain. *Nature* 447, 83–86.
- Wang, L., Zhu, C., He, Y., Zang, Y., Cao, Q., Zhang, H., Zhong, Q., Wang, Y., 2009. Altered small-world brain functional networks in children with attention-deficit/hyperactivity disorder. *Hum. Brain Mapp.* 30, 638–649.
- Wespatat, V., Tennigkeit, F., Singer, W., 2004. Phase sensitivity of synaptic modifications in oscillating cells of rat visual cortex. *J. Neurosci.* 24, 9067–9075.

- Womelsdorf, T., Schoffelen, J., Oostenveld, R., Singer, W., Desimone, R., Engel, A.K., Fries, P., 2007. Modulation of neuronal interactions through neuronal synchronization. *Science* 316, 1609-1612.
- Zang, Y.-F., He, Y., Zhu, C.-Z., Cao, Q.-J., Sui, M.-Q., Liang, M., Tian, L.-X., Jiang, T.-Z., Wang, Y.-F., 2007. Altered baseline brain activity in children with ADHD revealed by resting-state functional MRI. *Brain Dev.* 29, 83–91.
- Zhou, Y., Liang, M., Tian, L., Wang, K., Hao, Y., Liu, H., Liu, Z., Jiang, T., 2007. Functional disintegration in paranoid schizophrenia using resting-state fMRI. *Schizophr. Res.* 97, 194–205.
- Zijlmans, M., Huiskamp, G., Hersevoort, M., Seppenwoolde, J.-H., van Huffelen, A.C., Leijten, F.S.S., 2007. EEG-fMRI in the preoperative work-up for epilepsy surgery. *Brain* 130, 2343–2353.
- Zumer, J.M., Brookes, M.J., Stevenson, C.M., Francis, S.T., Morris, P.G., 2010. Relating BOLD fMRI and neural oscillations through convolution and optimal linear weighting. *Neuroimage* 49, 1479–1489.

Appendix A

2008-125::5:

AUP Number: 2008-125

AUP Title: Role of Frontal Cortex in Cognitive Control

Yearly Renewal Date: 02/01/2014

The YEARLY RENEWAL to Animal Use Protocol (AUP) 2008-125 has been approved, and will be approved for one year following the above review date.

1. This AUP number must be indicated when ordering animals for this project.
2. Animals for other projects may not be ordered under this AUP number.
3. Purchases of animals other than through this system must be cleared through the ACVS office. Health certificates will be required.

REQUIREMENTS/COMMENTS

Please ensure that individual(s) performing procedures on live animals, as described in this protocol, are familiar with the contents of this document.

The holder of this Animal Use Protocol is responsible to ensure that all associated safety components (biosafety, radiation safety, general laboratory safety) comply with institutional safety standards and have received all necessary approvals. Please consult directly with your institutional safety officers.

Submitted by: Kinchlea, Will D
on behalf of the Animal Use Subcommittee

The University of Western Ontario
Animal Use Subcommittee / University Council on Animal Care
Health Sciences Centre, • London, Ontario • CANADA – N6A 5C1
PH: 519-661-2111 ext. 86768 • FL 519-661-2028
Email: auspc@uwo.ca • <http://www.uwo.ca/animal/website/>

Curriculum Vitae

Name: Masoomeh Hashemi

Post-secondary Education and Degrees: Amirkabir University of Technology, Tehran Polytechnic
Tehran, Iran
2007-2011 B.Sc. Bioelectrical Engineering

University of Western Ontario
London, Ontario, Canada
2013-2015 M.Sc. Neuroscience

Honours and Awards: Western Graduate Research Scholarship (\$10,800 per annum):
2013-2014

Poster Presentation at Society for Neuroscience (SfN)
Washington, DC
11/2014

Poster Presentation at Unconventional Computation and Natural Computation (UCNC)
London, Ontario, Canada
07/2014
Neural correlates of spontaneous BOLD fluctuations: A simultaneous LFP-fMRI investigation in the nonhuman primate

Neuroscience Councilor for Society Of Graduate Students (SOGS)
University of Western Ontario
2013-2014

Ranked 600 among more than 500,000 participants in the Iranian national universities entrance exam

Related Work Experience Teaching Assistant
University of Western Ontario
2013-2014

Biomedical Technician
Milad Hospital, Tehran, Iran
2010

Research Experience Research Assistant
Robarts Research Institute, University of Western Ontario
2013-2014

Researcher
Science Beam Institute, Tehran, Iran
2011-2012

Additional Training Animal Care and Handling Certificate
Basic Handling, Sterile Injection Techniques
Care and Use of Non-Human Primates
University of Western Ontario
2013-2014

Publications:

Hutchison, R. M., Hashemi, N., Gati, J. S., Menon, R. S., Everling, S. 2015.
Electrophysiological signatures of spontaneous BOLD fluctuations in macaque prefrontal cortex. *NeuroImage* 113. 257-267.